PHOSPHO-ADDUCIN DISTRIBUTION IN A MURINE TRANSGENIC MODEL OF AMYOTROPHIC LATERAL SCLEROSIS

by

Xiao Yang Shan
M.D., Guangxi Medical University, 1989
M.Sc., Guangxi Medical University, 1997

THESIS SUBMITTED IN PARTIAL FULFILLMENT OF
THE REQUIREMENTS FOR THE DEGREE OF

MASTER OF SCIENCE

In the School
of
Kinesiology

SIMON FRASER UNIVERSITY

Spring 2005

APPROVAL

Name: **Xiao Yang SHAN**

Degree: Master of Science

Title of Thesis: Phospho-Adducin Distribution in a Murine Transgenic Model of Amyotrophic Lateral Sclerosis

Examining Committee:

Chair: **Dr. John Dickinson**
Professor

Dr. Charles Krieger
Senior Supervisor
Professor, School of Kinesiology

Dr. Neil Watson
Supervisor
Associate Professor, Department of Psychology

Dr. Nicholas Harden
Supervisor
Associate Professor, Department of Molecular Biology and Biochemistry

---

Dr. Wade Parkhouse
External Examiner
Professor, School of Kinesiology
Simon Fraser University

Date Approved: 10th March 2005

SIMON FRASER UNIVERSITY

PARTIAL COPYRIGHT LICENCE

Abstract

Amyotrophic lateral sclerosis (ALS) is a human neurodegenerative disorder characterized by the selective death of neurons in spinal cord, brain stem and cortex. The pathogenesis of ALS is still unknown. Adducins (Add) are a family of cytoskeletal associated proteins. Recent studies have shown that protein levels of phosphorylated adducin (phospho-adducin, p-Add) are increased in spinal cord tissue from ALS patients.

I have evaluated the distribution of p-Add immunoreactivity in spinal cords of mice over-expressing mutant human superoxide dismutase (mSOD), an animal model of ALS, and in control littermates. Spinal cords of mSOD mice having motoneuron loss exhibit significantly greater p-Add immunoreactivity in ventral horn and dorsal horn, compared to control animals.

The findings demonstrate increased immunoreactivity of phosphorylated adducin in a murine model of ALS. This increased p-Add immunoreactivity may be evidence for aberrant phosphorylation events contributing to motoneuron loss in mSOD mice.

Dedication

I dedicate this thesis

to my parents and my wife for their constant encouragement and love.

Acknowledgements

I am deeply indebted to my senior supervisor, Dr. Charles Krieger, for his expert guidance, advice, supervision as well as the encouragement and stimulating discussions through out the course of my study. He has not only led me into the exciting research field of neuroscience but has also shown me the right way and attitude of doing research. What I have learnt from him will benefit my career and life in the future.

I would also like to extend my sincere gratitude and appreciation to:

Dr. Neil Watson and Dr. Nicholas Harden (external supervisors), for their editorial insights and expert assistance in neuroanatomy and protein biochemistry.

Dr. Wade Parkhouse (external examiner), for his critical review and constructive opinions on this thesis.

Thanks to all above of you not just for being on my committee but for all of your nice guidance in many aspects.

Professor Parveen Bawa and Professor John Dickinson, for their kindness, support and wise advice during the course of my study.

Dr. Francisco Cayabyab, for his excellent technical assistance of TPLSM imaging and sharing knowledge in many ways.

Professor Guiying Zhou and Professor Jianning Jiang from Guangxi Medical University, for their abundant encouragement.

The staff in the Kinesiology office, Shona and Marilyn, for their administrative support and friendship; the staff of Animal Care Facility for their assistance on my transgenic mouse model.

My many student colleagues, Jiehong Hu, Xuan Geng, Lori Cunningham, Jennifer Litt, Ingrid Mcfee, Jennifer Solomon, Perveen Biln and Dwayne Hamson, for their friendship. Also to Dr. Tao Peng, my best friend in medical school, for helping me get through the difficult times and all the moral support he provided.

Finally, I am grateful to the members of my family, my beloved parents and my uncle, my wife, Yongchun, and my daughters, Jiabao and Jiaxin, for their everlasting love and understanding, with which I went through all tough time at Academy.

Table of Contents

Approval ii

Abstract iii

Dedication iv

Acknowledgements v

Table of Contents vi

List of Figures viii

List of Tables x

List of Abbreviations xi

1 Introduction 1

1.1 Amyotrophic lateral sclerosis (ALS) 1
1.2 Adducin and its role in nervous system 3
1.2.1 Adducin structure and genes 4
1.2.2 Regulation of adducin activities 6
1.2.3 Cellular and subcellular distribution of adducin in nervous system 10
1.3 Mutant SOD (mSOD) transgenic mouse model of ALS 12
1.3.1 SOD mutation and gain of toxic functions 12
1.3.2 Mutant SOD (mSOD) transgenic mouse model of ALS 14
1.3.3 Elevated phosphoprotein protein level in mSOD mice and in ALS 16

2 Rationale and Objective 19

2.1 Rationale 19
2.2 Objective 20

3 Materials and Methods 21

3.1 Chemical reagents 21
3.2 Animals 23
3.3 Animal genotyping 23
3.4 Preparation of spinal cord tissue 24
3.4.1 Perfusion and cryostat sectioning 24
3.4.2 Homogenization and protein concentration assay 25
3.5 Antibodies 26
3.6 Western blot analysis 27
3.7 Immunohistochemistry 28

3.8 Quantitative analysis of p-Add immunoreactivity 29
3.9 Confocal microscopy and imaging analysis 32

4 Results 33

4.1 Protein level of p-Add and adducin α and β in the spinal cords of mSOD mice 33
4.2 Phospho-adducin immunoreactivity in the control mouse 36
4.2.1 General observation 36
4.2.2 Central canal, white matter and dorsal horn 39
4.3 Phospho-adducin immunoreactivity in the mSOD mouse 42
4.4 Increased p-Add immunoreactivity in mSOD mice localizes to astrocytes 49
4.5 Subcellular locolization of p-Add in motoneurons 51

5 Discussion 59

5.1 Distribution of p-Add in control spinal cord 61
5.2 Phospho-adducin immunoreactivity in symptomatic mSOD mice 62
5.3 Elevated phosphoprotein immunoreactivity in mSOD mice and in ALS 63
5.4 What role does p-Add play in the mSOD mouse and in ALS? 64
5.5 Conclusions and future studies 66

Reference List 68

List of Figures

Figure 1-1: Putative model for p-Adducin action: Under resting conditions adducin links actin filaments to spectrin near the plasma membrane; When activated by PKC, p-Add dissociate from spectrin and actin and from the membrane to the cytosol (Gilligan et al., 2002), as well as inhibits the activity of adducin in promoting spectrin-actin complexes (Matsuoka et al., 1998). In this activation event, adducin is phosphorylated by PKC, and de-phosphorylated by myosin phosphatase (Kimura et al., 1998).....7

Figure 3-1: Quantification of p-Add immunoreactivity determined by sampling ROIs (60 x 60 pixels) in the regions of dorsal and ventral horns of spinal sections (open squares) and one ROI in the region of central canal (not shown). See Methods. 31

Figure 4-1: Protein level of p-Add by Western blot. A and B. No significant differences were found in the protein level of p-Add in spinal cord tissues from pre-symptomatic mSOD mice compared to littermate controls (A), or in mice at end-stage (B). Blots from affected animals and corresponding littermate controls are shown. Blots were normalized to actin. 34

Figure 4-2: Protein levels of Adducin α (A) and Adducin β (B) by Western blot. No significant differences were found in the protein levels of Adducin α and β in spinal cord tissues from symptomatic mSOD mice compared to littermate controls. Blots were normalized to actin. 35

Figure 4-3: Immunoreactivity to p-Add is present in motoneurons, ependyma and white matter. *A and B,* Sections of wild type mouse labeled for p-Add, *B* is magnified region of *A*. *C-H,* sections double labeled for p-Add (*red*; *C,F*) and MAP-2, a neuronal marker (*green*; *D,G*), co-localization as demonstrated by yellow color in *E, H.* Scale bars: *A,* 100μm; *B-H,* 50 μm.....38

Figure 4-4: Immunoreactivity to p-Add in ependyma and astrocytes. *A and B,* sections from wild type mice labeled with p-Add reveal immunostaining of ependyma using DAB and Cy3, respectively. *C-H,* sections double labeled for p-Add (*red*; *C, F*) and GFAP, an astrocyte marker (*green*; *D, G*), co-localization in the region of

ventral white matter (*C, D* and *E*) and dorsal horn (*F, G* and *H*) as demonstrated by yellow color in *E, H*. Scale bars: 50 μm. 41

Figure 4-5: Distribution of p-Add immunoreactivity in wild type and mSOD mice. Lumbar sections from wild type (left panels) and mSOD mice (right panels) immunolabeled with p-Add antibody. For DAB staining, *A* is lumbar section of wild type and *B* is mSOD spinal cord; *C* and *D* are magnified regions of ventral horn from *A* and *B*, respectively. For immunoreactivity for p-Add visualized by Cy3, *E* is from wild type and *F* from mSOD; *G* and *H* are magnified regions of ventral horn from *E* and *F*, respectively. Scale bars: *A, B, E and F*, 100μm; *C, D, G and H*, 50 μm 43

Figure 4-6: Relative quantification of p-Add immunoreactivity in lumbar spinal cords (mSOD n = 5, wild type n = 5). Overall effects were evaluated by multivariate analysis employing a repeated measures general linear model. Comparison between two groups were performed by independent t-tests, *P < 0.05, ** P < 0.01, respectively. P-Add immunoreactivity is increased significantly in both the ventral and the dorsal horn regions of mSOD mice compared to wild type littermate controls. 46

Figure 4-7: Immunoreactivity to p-Add in motoneuron axons. *A* and *B*, sections of wild type and mSOD mice labeled with p-Add. *C, D* and *E*, sections from mSOD mouse double labeled for p-Add (*red*; *C*) and SMI31, a marker for neurofilament (*green*; *D*), co-localization as demonstrated by yellow color in *E*. Scale bars: 50 μm. 48

Figure 4-8: The increase in p-Add immunoreactivity in mSOD mice localizes to the regions of increased GFAP immunoreactivity. *A, B* and *C* are sections from wild type mice; *D, E* and *F* are from mSOD mice. Sections were double labelled for p-Add (*red*; *A, D*) and GFAP, a marker for astrocytes (*green*; *B, E*), showed colocalization in the region of ventral horn (*C, F*) as demonstrated by *yellow*. Scale bars: 100 μm 50

Figure 4-9: Confocal images of the central canal of wild type and mSOD spinal cords. *A, C,* Z-stacked images of the central canal were used to reconstruct the 3D images projected on the y-axis. *B, D*, Single confocal images of the central canal showing expression of pAdd-immunoreactive products in the plasma membranes of ependyma. Spinal cords were labeled with p-Add primary and Cy3-conjugated secondary antibodies. Scale bars: 20 μm. 52

Figure 4-10: Confocal images of wild type and mSOD motoneurons. The 3D reconstructed images (projected in the y-axis, *A* and *C*) shows more p-Add labeling in mSOD spinal cords. Single confocal images (*B*

and *D*) show greater sub-plasma membrane staining of p-Add in mSOD. Scale bars: 20 μm. 54

Figure 4-11: The relative intensities of plasma membrane and cytosolic p-Add labeling in wild type and mSOD ventral horn motoneurons by obtaining line intensity profiles using LSM Image Examiner for each motoneuron. Again, it is showed that greater sub-plasma membrane staining of p-Add in mSOD compared to wild type mice (corresponding to the boxed motoneurons in Figure 10*B* and 10*D*, see Methods for details). 55

Figure 4-12: Two photon laser scanning microscopy (TPLSM) images of wild type and mSOD motoneurons and subcellular localization of p-Add immunoreactivity. *A*, Wild type motoneurons show polarized cytosolic localization of small (0.5-2 μm) puncta immunoreactive to the p-Add antibody. *B*, Ventral horn motoneurons of mSOD mice show less punctate immunoreactive products near perinuclear regions than controls, and some motoneurons show dispersed puncta and migration of p-Add immunoreactive products to sub-plasmalemmal domains. Spinal cords were labeled with p-Add. Scale bars: 20 μm. 57

List of Tables

Table 3.1: Reagents 21

List of Abbreviations

Add	adducin
ALS	amyotrophic lateral sclerosis
BSA	bovine serum albumin
CaMKK	Ca^{2+}/calmodulin-dependent protein kinase kinase
CDK	Cyclin-dependent kinase
CNS	central nervous system
Cy3	cyanine 3
DAB	diaminobenzidine tetrahydrochloride
DAG	diacylglycerol
DLN	dorsolateral nucleus
DMSO	dimethyl sulfoxide
DRG	dorsal root ganglion
EAA	excitatory amino acid
ECL	enhanced chemiluminescence
F-actin	actin filament
FALS	familial form of amyotrophic lateral sclerosis
FBS	fetal bovine serum
GDNF	glial-derived neurotrophic factor
GFAP	glial fibrillary acidic protein
GSK3α/β	glycogen synthase kinase 3 α/β
HRP	horseradish peroxidase
ICC	immunocytochemistry
IF	intermediate filament
Ig	immunoglobulin
IHC	immunohistochemistry
IHI	intracytoplasmic hyaline inclusion

IPC	insoluble protein complex
IR	immunoreactivity
LI	Lewy body-like inclusions
LTP	long term potentiation
MAP2	microtubule-associated protein 2
MARCKS	myristoylated alanine-rich C kinase substrate
MND	motoneuron disease
mSOD	mutant superoxide dismutase
NGF	nerve growth factor
NF	neurofilament
NFM	neurofilament middle chain
NFH	neurofilament heavy chain
NMDA	N-methyl-D-aspartate
OD	optical density
ON	Onuf's nucleus
p-Add	phospho-adducin
PBS	phosphate buffered saline
PBST	0.3% Trition X-100 in PBS
PCR	polymerase chain reaction
PFA	paraformaldehyde
PK	protein kinase
PKA	cAMP-dependent protein kinase
PKB	protein kinase B
PKC	protein kinase C
PMA	phorbol 12-myristate 13-acetate
PMSF	phenylmethylsulfonyl fluoride
PP	protein phosphatase
PSD	postsynaptic density
PSD-95	postsynaptic density protein 95
ROI	region of interest
RSK	ribosomal S6 kinase

S6K	S6 kinase
SALS	sporadic form of amyotrophic lateral sclerosis
SAPK	stress-activated protein kinase
SDS	sodium dodecylsulphate
SDS-PAGE	SDS-Polyacrylamide gel electrophoresis
Ser	serine
SNB	spinal nucleus of the bulbocavernosus
SOD1	Cu/Zn superoxide dismutase
TE	Tris-EDTA buffer
Thr	threonine
TPLSM	two-photon laser scanning microscopy
wt	wild type

1 Introduction

1.1 Amyotrophic lateral sclerosis (ALS)

Amyotrophic lateral sclerosis (ALS), also known as motoneuron disease (MND) or Lou Gehrig's disease, is a late onset neurodegenerative disease characterized by the selective death of motoneurons in spinal cord and brain stem, corticospinal tracts and other neurons (Eisen et al., 1998). The clinical features of ALS include progressive muscle weakness, muscle atrophy and eventual paralysis, ultimately, leading to death within 2–5 years of onset (Krieger et al., 1996).

The vast majority of ALS cases are sporadic (called sporadic ALS, or SALS) with no known genetic component. Familial ALS (FALS) is inherited in an autosomal dominant pattern and accounts for approximately 10% of all ALS cases. A subset of FALS cases (approximately 20 %) have mutations in the gene coding for superoxide dismutase 1 (SOD1) (Rosen et al 1993).

The causes for most cases of ALS are unknown and the clinical course is highly variable, suggesting that multiple factors might underlie the disease mechanism. Several causal hypotheses have been proposed including oxidative stress, glutamate excitotoxicity, protein aggregates, and aberrant protein kinase and phosphoproteins.

There is considerable interest in identifying proteins that might be responsible for the selective vulnerability of certain populations of neurons to disease. For instance, the presence of excitatory amino acid receptors and associated ligand-gated channels can lead to the death of neurons expressing these receptors following exposure to an appropriate ligand. Moreover, it is possible that the expression of certain structural proteins may also be relevant for the selective vulnerability of specific neuron populations.

One group of structural proteins that is of particular interest is the adducins. Adducins are a family of cytoskeletal-associated proteins that link spectrin and actin filaments in the regulation of cytoskeletal architecture, and form substrates for protein kinase C (PKC) and other signaling molecules (Gardner and Bennett, 1987; Matsuoka et al, 1996; Li et al., 1998; Matsuoka et al, 1998). This group of structural proteins is located predominantly in membrane regions highly enriched with synapses, suggesting that adducins are associated with neurotransmitter receptors (Matsuoka et al., 1998). Recent studies of protein kinase and phosphoprotein expression using multi-immunoblotting techniques have demonstrated that phospho-adducin (p-Add) is expressed in both murine and human spinal cord (Hu et al., 2003a; 2003b). Interestingly, the protein level of p-Add is significantly increased in spinal cord tissue from patients who died with ALS, compared to controls (Hu et al., 2003b). Previous studies of protein kinase activities and protein levels of PKC in ALS tissue have demonstrated significant elevations compared to control tissue (Lanius et al., 1995; Hu et al., 2003b). The explanation for the increased protein level of p-Add in spinal cord tissue from patients with ALS is unknown, but could result from increased phosphorylation of adducin by

PKC. It is also a mystery whether the increased protein level of p-Add has causative or protective roles in motoneuron death in ALS.

1.2 Adducin and its role in nervous system

Adducin α, β and γ are heteromeric proteins that cross-link actin with spectrin (Gardner and Bennett, 1987; Li et al., 1998), by bundling and capping actin filaments, and these proteins are widely expressed in many cell types including neurons and glial cells (Mische et al., 1987; Kuhlman et al., 1996). Adducin proteins are encoded by α, β and γ adducin genes, where there is a ubiquitous expression of α- and γ-adducin and a more restricted expression pattern of β-adducin (Gilligan et al., 1999).

Adducin is localized at spectrin-actin junctions in erythrocyte membrane skeletons (Derick et al. 1992) and colocalizes with spectrin at sites of cell–cell contact in epithelial cells (Kaiser et al., 1989; Hughes et al., 1995), and in the dendritic spines of hippocampal neurons (Seidel et al., 1995; Matsuoka et al, 1998). Adducin has been suggested to have several functions in vitro: it bundles actin filaments (F-actin) (Mische et al., 1987); caps the fast-growing ends of actin filaments (Kuhlman et al., 1996) and recruits spectrin to the fast-growing ends of actin filaments (Gardner and Bennett, 1987). Furthermore, adducin has demonstrated many physiological roles such as promoting platelet aggregation (Gilligan et al., 2002), maintaining membrane stability in red blood cells (Gilligan et al., 1999), and membrane ruffling and cell motility in MDCK cells (Fukata et al., 1999).

1.2.1 Adducin structure and genes

Adducins are a family of cytoskeletal associate proteins encoded by three related genes: *ADD1, ADD2*, and *ADD3*. Functional adducin is a heteromeric protein comprised of either α and β, or α and γ subunits (Dong et al., 1995; Hughes et al., 1995). α and γ adducin are expressed in all mouse and human tissues, whereas β adducin has a more restricted pattern of expression in brain and erythropoietic tissues (Joshi et al., 1991, Gilligan et al., 1999). All three adducin subunits contain three structurally distinct domains: a 39 kD NH2 -terminal globular head domain, connected by a 9-kD neck domain to a 33-kD C-terminal tail domain with the spectrin/actin interaction site (Joshi et al., 1990, 1991; Hughes et al., 1995; Li et al., 1998).

The C terminal domain of all three subunits of adducin contains a 22 amino acid-residue with sequence similarity to a domain in the myristoylated alanine-rich C kinase substrate (MARCKS) (Joshi et al., 1991; Dong et al., 1995). The MARCKS-related domain is required for interactions of adducin with actin and spectrin (Li et al., 1998). The MARCKS-related domain also has a major phosphorylation site, the RTPS-serine, for PKC as well as cyclic AMP (cAMP)-dependent protein kinase (PKA), and contains the primary calcium/calmodulin-binding site of adducin (Matsuoka et al., 1996; 1998).

The *ADD1, ADD2*, and *ADD3* genes belong to a gene family and map onto different chromosomes, encoding polypeptides of 737, 726 and 706 amino acids, respectively (Joshi et al., 1991; Citterio et al., 1999). The primary sequences of α and β adducin display 49% identity and 66% similarity at the amino acid level. γ adducin shares 60–70% sequence similarity with both α and β adducin. A very high homology exists

between rat and human adducin genes with ~91% amino acid identity (Joshi et al., 1991; Citterio et al., 1999). Alternative splicing of adducin mRNA results in truncated polypeptide isoforms (called α-2, β-2 and γ-2, respectively) and these are very common in the adducin family with a majority of transcript variants for the *ADD2* gene (Gilligan et al., 1997; Suriyapperuma et al., 2000).

Human *ADD1* has been mapped by positional cloning to human chromosome 4p16.3 (Goldberg et al., 1992). The human α adducin gene contains 16 exons and spans about 85 kb of genomic DNA (Lin et al., 1995). Two alternatively spliced isoforms of α adducin have been identified. A 93-bp is inserted in frame between codons 471 and 472 and a 34-bp inserted within codon 621 comprising exon 15 disrupts the reading frame and introduces a stop codon after 11 novel amino acids (Goldberg et al., 1992).

Human *ADD2* has 13 exons and is localized to chromosome 2p13 (Gilligan et al., 1995). Isoforms of β adducin can be divided into two groups. Members of one group all contain the MARCKS-related domain, whereas members of the other group lack this domain (Tisminetzky et al., 1995; Suriyapperuma et al., 2000).

Human *ADD3* gene spanning over 20 kb has been mapped to chromosome 10q 24.2-24.3 (Katagiri et al., 1996) and is composed of at least 13 introns and 14 exons covering the entire coding region. *ADD3* presents only one variant containing an in-frame exon insertion encoding a longer protein (Citterio et al., 1999; Suriyapperuma et al., 2000)

There is a high degree of conservation of polypeptide sequences across species, and several domains are highly conserved among α, β and γ isoforms, suggesting that *α, β*

and γ genes arose from gene duplication (Suriyapperuma et al., 2000). In particular, the C terminal region involved in spectrin-actin binding is highly conserved in the α-1, β-1 and γ-1 isoforms, suggesting that αβ and αγ heterodimers may have similar functions although expressed in different cells. However, the truncated isoforms, α-2 and β-2 are missing the spectrin-actin binding domain of the α-1and β-1 isoforms, suggesting that they have different functions which remain to be determined (Suriyapperuma et al., 2000).

1.2.2 Regulation of adducin activities

Phosphorylation of cytoskeletal proteins occurs *in vivo*, and this post-translational modification can alter the properties of these substrate proteins leading to important functional consequences. The interaction of adducin with spectrin and actin is regulated by calcium and calmodulin (Gardner and Bennett, 1987), and by several protein kinases through phosphorylation, such as protein kinase C (PKC), cyclic AMP-dependent protein kinase, (protein kinase A, PKA), Fyn, and rho-associated kinase (rho-kinase) (Bennett et al., 1988; Matsuoka et al, 1996; Kimura et al., 1998; Matsuoka et al, 1998; Fukata et al., 1999; Shima et al., 2001). (Figure 1-1)

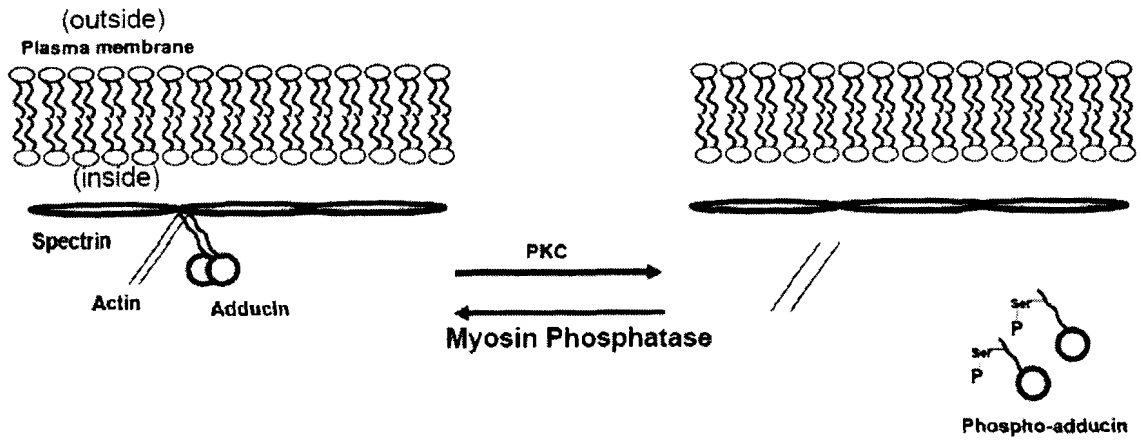

Figure 1-1: Putative model for p-Adducin action: Under resting conditions adducin links actin filaments to spectrin near the plasma membrane; When activated by PKC, p-Add dissociate from spectrin and actin and from the membrane to the cytosol (Gilligan et al., 2002), as well as inhibits the activity of adducin in promoting spectrin-actin complexes (Matsuoka et al., 1998). In this activation event, adducin is phosphorylated by PKC, and de-phosphorylated by myosin phosphatase (Kimura et al., 1998).

1.2.2.1 PKC

Protein kinase C represents a family of calcium and phospholipid-dependent enzymes which catalyzes the covalent transfer of phosphate from ATP to serine and threonine residues on proteins. The phosphorylation of the substrate proteins induces a conformational change and thereby a modification of their functional properties (Parekh et al., 2000). The PKC family consists of at least 12 isoforms, which have been grouped into three subclasses according to their regulatory properties. The 'conventional' or 'classical' PKCs (cPKCs), including PKCα, β1, β2, and γ, can be activated by calcium and/or by diacylglycerol (DAG) and phorbol esters. The 'novel' PKCs (nPKCs) δ, ε, θ, η and μ can also be activated by DAG and phorbol esters but are calcium-independent. Finally, the atypical PKCs (aPKCs), which include PKCζ and PKCι (its mouse homologue has been named PKCλ), are unresponsive to calcium and DAG/phorbol esters.

PKC plays an important role in adducin activities. Adducin is phosphorylated by PKC *in vitro* and *in vivo* (Matsuoka et al., 1996 and 1998). Matsuoka et al., (1998), have observed that phospho-adducin immunocytochemistry was enhanced in human erythrocytes after treatments with PMA. The RTPS-serine (ser726 in adducin α, ser713 in β-adducin and ser662 in γ-adducin) of the MARCKS-related domain is a ser/thr phosphorylation site for PKC (Matsuoka et al., 1998). Phosphorylation of adducin by PKC induces translocation of phospho-adducin from the membrane to the cytosol (Kaiser et al., 1989; Gilligan et al., 2002), as well as inhibits the activity of adducin in promoting spectrin-actin complexes (Matsuoka et al., 1998).

1.2.2.2 PKA

PKA also phosphorylates adducin in vitro and downregulates actin-binding and spectrin-recruiting activities (Matsuoka et al., 1996). Ser726 and Ser713 are the common phosphorylation site for PKA and PKC. PKA, in addition, phosphorylates α adducin at Ser408, Ser436 and Ser481 (Matsuoka et al., 1996). Similarly, the phosphorylation of adducin by PKA reduces the ability of adducin to associate with F-actin and spectrin-F-actin complexes and to promote the binding of spectrin to F-actin. Although PKA phosphorylates adducin in vitro, it has not been established whether PKA phosphorylates adducin in vivo (Matsuoka et al., 1998).

1.2.2.3 Rho

Rho is a small GTPase that exhibits both GDP/GTP binding and GTPase activities. Rho has GDP-bound inactive (GDP-Rho) and GTP-bound active (GTP-Rho) forms, which are interconvertible by GDP/GTP exchange and GTPase reactions (Nobes et al., 1994; Ridley 1996) When cells are stimulated with certain extracellular signals such as lysophosphatidic acid, GDP-Rho is thought to be converted to GTP-Rho, which binds to specific targets and then exerts its biological functions. Rho activates Rho-associated kinase (Rho-kinase), which participate in signaling pathways that regulate actin cytoskeletons such as stress fibers and in cell-substratum adhesions such as focal adhesions in fibroblasts (Ridley et al, 1992).

Adducin has been identified by Kaibuchi and colleagues (Kimura et al., 1998) as a substrate for the Rho-kinase at a phosphorylation site distinct from PKC. The phosphorylation of α adducin by Rho-kinase occurs mainly on the threonine residue

(Thr445 and Thr480) of the neck domain of adducin. In contrast to PKC and PKA, the α adducin phosphorylated by Rho-kinase is co-sedimentated with F-actin more efficiently than the non-phosphorylated α adducin. Moreover, phospho-adducin is de-phosphorylated by myosin phosphatase (Kimura et al., 1998). These results suggested that Rho-kinase and myosin phosphatase regulate the phosphorylation states of adducin and that the increased phosphorylation of adducin by Rho-kinase stimulates the F-actin binding activity of adducin. This action of adducin may promote spectrin-actin complex formation at sites of cell-cell contact in epithelial cells (Kaiser et al., 1989). Experiments with mutated forms of adducin lacking the Rho-phosphorylation site suggest that Rho-dependent phosphorylation of adducin plays an essential role in promoting cell motility (Fukata et al., 1999).

1.2.2.4 Calcium/calmodulin

Calcium/calmodulin inhibits adducin activities in both actin-capping and spectrin-recruiting (Gardner and Bennett, 1987; Kuhlman et al., 1996). The major calmodulin binding site in adducin is localized at the MARCKS-related domain, which contains the common phosphorylation site for PKA and PKC (Matsuoka et al., 1996).

1.2.3 Cellular and subcellular distribution of adducin in nervous system

Only a limited number of studies have examined the distribution of adducin immunoreactivity in the nervous system. Seidel and colleagues (1995) studied the spatial and subcellular localization of α-adducin in rat brain and found that α-adducin is highly localized to regions with high synapse densities, such as the hippocampus, cerebral cortex

and cerebellum. The sub-cellular localization of α-adducin in hippocampus and cerebellum includes the dendrites and dendritic spines of neurons in the CA1 and CA3 regions of the hippocampus. Immunolabelling of α-adducin is also found in the pre-synaptic terminals of parallel fibers in the molecular layer of the cerebellum (Seidel et al., 1995). Seidel et al (1995) also found significant immunolabelling of α-adducin in the processes of glial cells, both in the hippocampus and cerebellum. Adducin β1 is highly expressed in cerebellum and dorsal root ganglia (DRG) tissues of rat and can be developmentally up-regulated by trophic factors like nerve growth factor (NGF) and glial-derived neurotrophic factor (GDNF) (Ghassemi et al., 2001). Moreover, the α-isoform of adducin is also present in the postsynaptic densities (PSD) regions of rat brain (Wyneken et al., 2001). Furthermore, Matsuoka et al. (1998) observed that RTPS-serine phosphorylation of adducin was present in postsynaptic areas in the developing rat hippocampus, and in the dendritic spines of cultured hippocampal neurons.

Based on the known function of adducin so far, these findings suggest that adducin has effects on the structure of dendritic spines, and might have a functional interaction with receptors which integrate with postsynaptic cytoskeleton in dendritic spines. Actin filaments are highly concentrated in the post-synaptic density (PSD), and actin depolymerization reduces NMDA channel activities on cultured hippocampal neurons (Rosenmund et al., 1993). However, the distribution of adducins and p-Add immunoreactivity in spinal cord has not been examined either in ALS patients or any murine model of ALS, and subcellular localization of adducins and p-Add is also unknown.

1.3 Mutant SOD (mSOD) transgenic mouse model of ALS

1.3.1 SOD mutation and gain of toxic functions

More than 100 mutations have been identified in the *sod1* gene in 20% patients with FALS, and all mutations cause dominantly inherited disease except one mutation, D90A mSOD (Andersen 2000; Andersen et al., 2001). Wild type (wt) Cu/Zn superoxide dismutase (SOD1), a homodimer of a ubiquitously expressed 153–amino acid polypeptide, functions to convert superoxide radical (O_2-), a toxic by-product of mitochondrial oxidative phosphorylation, to water or hydrogen peroxide (H_2O_2) (McCord and Fridovich, 1969; Brunori and Rotilio, 1984). The exact mechanisms underlying neuronal death induced by mSOD are still unclear.

It was initially thought that the toxicity of different SOD1 mutants could result from the observations of a 25-50% reduction of total cellular SOD1 activity in FALS patients with a SOD1 mutation (Robberrecht et al., 1994, Bowling et al., 1995). A loss of normal dismutase function as a major factor in FALS was further supported by the observation that down-regulation of SOD1 leads to the apoptotic degeneration of PC12 cells (Troy et al., 1994) or spinal cord neurons in organotypic culture (Rothstein et al., 1994). However, most recent studies have not supported this view. For instance, SOD1 null mice did not develop motor neuron disease (Reaume et al., 1996). Transgenic mice expressing mutants SOD1G93A or SOD1G37R developed motor neuron disease despite elevation in SOD1 activity levels (Cleveland, 1999). Some mutant enzymes retain full dismutase activity (Borchelt et al. 1994, Bowling et al. 1995). Furthermore, an increase in the dismutase activity has no effect on disease (Bruijn et al. 1998).

Currently, it is believed that SOD1-mediated toxicity in ALS is not due to loss of function but instead to a gain of toxic functions that are independent of the levels of SOD1 activity. Aberrant copper-mediated catalysis of mSOD has been extensively studied. One hypothesis is that misfolding of mSOD would use abnormal substrates such as nitric oxide (NO) to the catalytic site to generate peroxynitrite leading to the nitration of tyrosine residues, thus damaging proteins in affected cells (Beckman et al., 1993). This hypothesis is supported by the increased levels of free 3-nitrotyrosine detected in the spinal cord of human ALS patients (Beal et al., 1997) and in mouse models of ALS (Bruijn et al., 1997a). However, there is no evidence of increased levels of nitrotyrosine bound to proteins in ALS patients or in mSOD mice (Bruijn et al., 1997a; Strong et al., 1998). Furthermore, using mass spectrometry, Williamson et al. (2000) detected no increased nitration in neurofilaments isolated from transgenic mice expressing dismutase-active or -inactive mutants.

Another possible inappropriate enzymatic substrate for mSOD is its own normal end product hydrogen peroxide. Use of hydrogen peroxide by mSOD may generate toxic free radicals such as hydroxyl that can damage cellular targets including DNA, protein, and lipid membranes (Wiedau-Pazos et al., 1996). This possibility has been supported by observations of elevated hydroxyl radical-like activity in G93A mSOD mice (Bogdanov et al., 1998; Ferrante et al., 1997a) and of oxidative damage in neuronal tissue of sporadic and familial ALS (Ferrante et al., 1997b). However, increase in hydroxyl radicals has not been detected in other mouse models (Bruijn et al., 1997a). Thus, there is no consensus regarding the mechanisms of disease involving superoxide-mediated oxidative damage in ALS.

There is also considerable evidence that mSOD produces aggregates that may affect the function of neurons and other cells (Durham et al., 1997; Bruijn et al., 1998; Johnston et al., 2000; Price et al., 2000; Wang et al., 2002; Agar et al., 2003). Prominent intracellular cytoplasmic inclusions in motor neurons and in some cases within the astrocytes surrounding them are found in mSOD mouse models of ALS and in some tissue from patients with ALS (Bruijn et al. 1998). These aggregates found in motoneurons and astrocytes of mSOD mouse models of ALS are highly immunoreactive for SOD1 (Bruijn et al., 1997b; 1998). Also, there is intense SOD1 immunoreactivity present in the intracytoplasmic hyaline inclusions (IHIs) of the ventral horn cells from ALS patients at autopsy (Shibata et al., 1996). Some mSOD aggregates form insoluble protein complexes (IPCs) in motoneurons from mSOD transgenic mice or cultured motoneurons expressing mSOD (Tu et al., 1996; Durham et al., 1997; Bruijn et al., 1998; Johnston et al., 2000). Hypotheses of toxicities of the protein aggregates include aberrant chemistry, loss of protein function through coaggregation, depletion of protein folding chaperones, loss of proteasome function, and mitochondria damage (see review, Bruijn et al., 2004).

1.3.2 Mutant SOD (mSOD) transgenic mouse model of ALS

Mice over-expressing human mutant SOD1 (mSOD) transgenes have been used to study the role of mSOD in motoneuron death. Lines of mice overexpressing human mutant SOD1 (G85R, G37R, and G93A) have been extensively characterized as models of ALS (Bruijn & Cleveland 1996, Gurney 1994, Wong et al.1995). It is known that in mSOD transgenic mice, the age of onset of the disease, the severity of pathological

abnormalities and clinical features are crucially depended on the copy numbers of the mutant transgene, or on the specific mSOD mutation (Wong et al., 1995; Dal Canto et al., 1997; Pramatarova et al., 2001). Comparative studies reveal a striking similarity in pathology between the mSOD mouse and human ALS, which include the loss of motoneurons, muscle atrophy, and the presence of large numbers of vacuoles and protein aggregates in the axons and perikaryal regions of motoneurons (Wong et al., 1995; Gurney et al., 1994).

The G93A mSOD transgenic mouse model is one of the most commonly used mouse models of ALS. Mice that over-express mSOD (G93A; line G1H) by 10-20 fold remain clinically asymptomatic until around 100 days of age when they manifest hind limb weakness that results in a slow, unstable gait (Gurney et al., 1994). However, animals are still able to ambulate, to feed, and to right themselves for about 3 weeks thereafter. By day 120-125 many are unable to right themselves and have difficulty feeding (Gurney et al., 1994; Hamson et al., 2002). These G93A mice are a good model of ALS; the mSOD mutation is detected in patients with FALS and the specific mSOD mutation in these mice correlates with disease onset and the rate of progression, as in ALS (Gurney et al., 1994). Furthermore, as in ALS, selective neuron vulnerability is seen in these G93A mice. In ALS, there is variable involvement of motoneurons, and descending motor fibres such as the corticospinal, bulbospinal and rubrospinal tracts. There is also variable involvement of frontal regions in ALS patients (see Eisen & Krieger, 1998). Remarkably, mice over-expressing mSOD also demonstrate similar motor system defects in both motoneurons and descending motor tracts (Zang & Cheema, 2002). Hamson et al (2002) have found that the spinal nucleus of the bulbocavernosus

muscle (SNB), a homologous structure to the nucleus of Onuf in humans, is spared in mSOD mice, paralleling observations in patients with ALS (Hamson et al., 2002). Sparing of motoneurons innervating extraocular muscles has been reported in these mice, again paralleling observations in ALS tissue (Haenggeli & Kato, 2002).Generally, a reduction of motoneuron numbers by 40-60% are seen in mSOD mice at 'end-stage' (Mohajeri et al., 1998; Hamson et al., 2002). These reductions in motoneuron number are similar to the extent of motoneuron loss in ALS patients at autopsy (Tsukagoshi et al., 1979).

1.3.3 Elevated phosphoprotein protein level in mSOD mice and in ALS

The increase in protein level of many phosphoproteins and protein kinases have been found in mSOD mice compared to wt littermates and in nervous system tissue from ALS patients, compared to controls. For instance, in a recent study, Hu et al (2003b) observed that elevated protein level and/or activation of many protein kinases in ALS tissue. These protein kinases included PKCα, PKCβ, PKCζ and GSK3α/β, which may augment neural death in ALS, and CaMKK, PKBα, Rsk1, S6K, and SAPK, which may be a response to neuronal injury that potentially can mitigate cell death. Furthermore, aberrant hyperphosphorylation of the microtubule-associated protein, tau, has been found both in a mouse model of ALS over-expressing human mutant SOD (G37R; Farah et al., 2003), and in frontal cortex tissue from patients who died from ALS, especially those that manifested cognitive impairment (Yang et al., 2003). The hyperphosphorylation of tau may be linked to increased protein level of CDK-5, which has also been reported in mSOD over-expressing mice (Nguyen et al., 2001). Additionally, p38α, a member of the

stress-activated protein kinase family, has been found to be associated with the abnormally phosphorylated side arms of neurofilament heavy and neurofilament middle proteins in ALS tissue, as well as in mice over-expressing human mutant SOD (Ackerley et al., 2004).

It has been previously proposed that the finding of hyperphosphorylation of a number of phosphoproteins in ALS tissue could also be the result of impaired activation of one or more protein phosphatases (Wagey et al., 1997). Protein phosphatases are responsible for the de-phosphorylation of protein kinases or phosphoproteins. Although the previously reported findings were consistent with this hypothesis (Wagey et al., 1997), more recent observations have not demonstrated impairments in the activation and protein content of the protein phosphatase, calcineurin, in mSOD mice (Li et al., 2004).

The presence of increased expression of a number of phosphoproteins in mSOD mice suggests that up-regulation of phosphorylation is a more general feature of this neurological disorder (Krieger et al., 2003). However, it is not clear if this increase in phosphorylation activity is a consequence of neuronal destruction, or reflects the action of regenerative mechanisms.

For example, the abnormal accumulation of neurofilaments in the perikaryon and axon of affected motoneurons, is a common pathological feature in both SALS and FALS (Hirano et al., 1984; Rouleau et al., 1996). Many of these accumulations label with antibodies that detect phosphorylated neurofilament middle chain (NFM) and neurofilament heavy chain (NFH) side-arms (Schmidt et al., 1987; Sobue et al., 1990). Similarly, neurofilament pathologies are also detected in mSOD mice (Nguyen et al.,

2001; Tu et al., 1996). However, the function of NFM and NFH side-arm phosphorylation is unclear. Many studies suggest that it is a regulatory mechanism for controlling the speed of transport of neurofilaments into and through axons; increased phosphorylation is associated with a slowing of transport (Ackerley et al., 2000, 2003; Jung et al., 2000). Slowing of neurofilament transport is an early pathological feature in several transgenic mouse models of ALS including those caused by mutant SOD1 (Collard et al., 1995; Williamson and Cleveland, 1999). In contrast, the perikaryal inclusion of hyper-phosphorylated NF proteins was suggested to confer protection by acting as a sink for abnormal protein phosphorylation (Nguyen et al., 2001). All together, a possible explanation is proposed that a disruption of axon transport by aberrant NF assembly is pathogenic in ALS, while the perikaryal NF accumulations have a beneficial role in motoneuron survival (See review: Julien, 2001; Al-Chalabi and Miller, 2003).

2 Rationale and Objective

2.1 Rationale

There is considerable interest in identifying proteins that might be associated with the selective vulnerability of certain populations of neurons to disease. One group of structural proteins that is of particular interest is the adducins. Using a multi-immunoblotting analysis, elevated protein level of p-Add and other phosphoproteins have been found in thoracic spinal cord tissue from patients who died with ALS, compared to controls, and the increase in p-Add protein level was the largest of any of the 31 phosphoproteins studied (Hu et al., 2003b). Adducins are located predominantly in membrane regions highly enriched with synapses, as well as in glial cells (Seidel et al., 1995). Furthermore, previous studies have also observed significantly increased protein level and activation of PKC isoforms in spinal cord tissue from ALS patients compared to controls (Lanius et al., 1995; Hu et al., 2003b). As PKC phosphorylates adducin at the MARCKS-related domain, these data suggest that one action of the elevated PKC activity in ALS tissue may be the phosphorylation of adducin. However, it is unknown what role does this p-Add may play in ALS, and the distribution of adducin in spinal cord has not been investigated. G93A mSOD mice is one of the most commonly used mouse models of ALS, and has been extensively used in studying the pathogenesis of ALS since these mice exhibit similar motor weakness and pathology resembling what seen in human ALS (Gurney et al., 1994). The purpose of this thesis is to understand and compare the content

and localization of p-Add in spinal cords of G93A mSOD mice and wild type littermate control mice.

2.2 Objective

The primary objective is to examine the distribution of the p-Add in spinal cord of G93A mSOD mouse model of ALS. I postulate first, that the content of p-Add in spinal cords of mSOD mice will be increased compared to wild type littermate control mice. Secondly, I postulate that the distribution pattern of p-Add will be altered in spinal cords of mSOD mice, compared to controls, particularly in anatomical regions that are affected in this mutant mouse. Thirdly, I postulate that the subcellular localization of p-Add will be different in spinal motoneurons from mSOD mice compared to controls. Specifically, I expect that p-Add will be likely be in cytosolic locations as a result of translocation.

3 Materials and Methods

3.1 Chemical reagents

Table 3.1: Reagents

Regent Name	Source Company
2-Mercaptoethanol	CaledonBiotech
Acrylamide	Sigma
Agar	VWR
Aprotinin	Sigma
Bis-acrylamide	Sigma
Bovine serum albumin (BSA)	Sigma
Chelex	Bio-Rad
Diaminobenzidine tetrahydrochloride (DAB)	Vector Laboratories
Dimethyl sulfoxide (DMSO)	BDH
Ethanol	Fisher
Ethylene diamine tetraacetate disodium salt (EDTA)	Fisher
Ethylene glycol	Sigma
Formaldehyde	Gibco
Glucose	BDH
Glycerol	Sigma
Glycine	Sigma
Hydrochloric acid (HCl)	Fisher
Hydrogen peroxide (H_2O_2)	BDH
Leupeptin	Sigma
Magnesium chloride ($MgCl_2$)	Fisher
Magnesium sulfate ($MgSO_4$)	Fisher
Methanol	Fisher

Regent Name	Source Company
Nonfat dry milk	Bio-Rad
Normal goat serum	Gibco
IGEPAL (NP-40)	Sigma
Paraformaldehyde (PFA)	ACROS
PCR kit	Invitrogen
Pepstatin	Sigma
Permount	Fisher
Phenol:chloroform:isoamyl alcohol (25:24:1)	Ivitrogen
Phenylmethylsulphonylfluoride (PMSF)	Sigma
Phosphate buffered saline (PBS)	Gibco
Poly-D-lysine	Sigma
Poly-L-lysine	Sigma
Polyvinylpyrrolidone (PVP-40)	Sigma
Potassium chloride (KCl)	Fisher
Protein assay reagent	Bio-Rad
Proteinase K	Invitrogen
Rnase	Sigma
Sodium azide (NaN_3)	Fisher
Sodium chloride (NaCl)	Fisher
Sodium dihydrogen phosphate (NaH_2PO_4)	BDH
Sodium dodecylsulphate (SDS)	Sigma
Sodium fluoride (NaF)	Sigma
Sodium hydrogen carbonate ($NaHCO_3$)	BDH
Sodium hydroxide (NaOH)	Fisher
Sodium orthovanadate (Na_3VO_4)	Sigma
Sucrose	BDH
Tetramethylethylenediamine(TEMED)	Bioshop
TrizmaBase	Sigma
Tween-20	Bio-Rad

3.2 Animals

Transgenic mice over-expressing human mutant SOD1 protein (G93A mSOD mice) were bred from progenitor stock obtained from the Jackson Laboratory (Bar Harbor, ME; strain B6SJL-TgN (SOD1-G93A)1Gur; Gurney et al., 1994). The mSOD expression was confirmed by a PCR-based assay (details see 3.3). Animals were treated in accordance with the requirements of the SFU Animal Care Committee and the Canadian Council for Animal Care. Mice were monitored closely following the onset of clinical symptoms and sacrificed at a pre-determined end-point based on the appearance of a set of behavioral markers (including hind limb ataxia, and an inability to forage due to paralysis of the hindlimbs including an inability to right themselves after 10 seconds of recumbency, so-called 'end-stage disease'), which occurs at 121.8 $\pm$ 2.0 days (mean $\pm$ SEM, n=18). Age-matched wild type littermates that were phenotypically normal and PCR assay negative served as controls.

3.3 Animal genotyping

The genotype of the mSOD mice were determined by appropriate PCR procedures with mouse genomic DNA as a template to amplify the 236 bp product from exon 4 of the human sod1 gene at 35 days of age. Genomic DNA was extracted from clipped mouse ear tissue and incubated in a mixture of Chelex (5% w/v), Proteinase K (2 mg/mL) and RNase (1 mg/mL), followed by extracting with phenol:chloroform:isoamyl alcohol (25:24:1) and precipitating with ethanol. The genomic DNA pellet was air dried, then dissolved in Tris-EDTA buffer (TE, pH 8.0) and stored at –20 oC before use as template. The PCR reaction was performed in 25 µl volumes containing 2.5µl of 10x

buffer (15 mM $MgCl_2$), 0.5 µl of each primer, 2.5 µl of dNTPs, 0.3 µl of Taq DNA polymerase and 1µl of genomic DNA. Samples were denatured for one cycle at 95°C for 5 minutes, followed by 30 cycles at 94°C for 30 s, 58°C for 30 s, and 72°C for 30 s; and a final extension at 72 °C for 10 min. The forward and reverse primers used are CATCAGCCCTAATCCATCTGA and CGCGACTAACAATCAAAGTGA, respectively. The detection of PCR product was performed by running a 1 % agarose gel electrophoresis.

3.4 Preparation of spinal cord tissue

3.4.1 Perfusion and cryostat sectioning

Experimental animals (n= 8) and littermate controls (n= 8) were sacrificed using progressively increasing CO_2 and O_2, to minimize animal distress, and rapidly perfused transcardially with 35 ml phosphate buffered saline (0.1M PBS, pH 7.4) followed by freshly prepared 35 ml 4% paraformaldehyde (PFA; pH 7.4). Spinal cords were dissected out, post-fixed in 4% PFA for 24 h, transferred to a 20% sucrose/ PBS solution overnight for cryoprotection, frozen in Tissue-Tek O.C.T compound (Sakura, Zoeterwoude, Netherlands) and sectioned in the transverse plane at 50 µm on a cryostat. Sections were suspended in Eppendorf tubes containing DeOlmos solution (Watson et al., 1986) for antigen protection and stored at -20^{0}C until processed for immunohistochemistry. Generally, lumbosacral regions of spinal cord were used for study, as these regions are prominently affected in mSOD mice (Gurney et al., 1994).

3.4.2 Homogenization and protein concentration assay

To quantify the total protein level of p-Add in spinal cords of pre-symptomatic (10 weeks of age) and 'end-stage' mice (17-19 weeks of age), mSOD (n=4) and age-matched wt littermate controls (n=4) were sacrificed as above. The spinal cords were rapidly removed and frozen at –80° C. Mice aged 10 weeks were chosen for study in the pre-symptomatic group as mSOD mice were very early in the course of their disease and likely did not manifest much neuropathological evidence of motor neuron disease.

Whole spinal cord protein lysates were obtained by homogenizing tissue in a RIPA lysis buffer containing 0.5% Nonidet P-40, 50mM Tris-HCl (pH 8.0), 150mM NaCl, 1mM EDTA and phosphatase/protease inhibitors including 1 μg/mL aprotinin; 1 μg/mL leupeptin; 1 μg/mL pepstatin; 1mM phenylmethylsulfonyl fluoride; 2mM activated sodium orthovanadate, 1mM sodium fluoride; followed by sonication with a Janke & Kunkel IKA Laortechnik Ultra-Turrax homogenizer. Homogenized tissues were subsequently centrifuged at 3,000 rpm for 5 minutes, and supernatant was centrifuged again at 12,000 rpm for 15 minutes at 4°C. The supernatant was stored at -80°C until further use.

Protein concentrations of tissue samples were determined by Bradford assay. A series of protein standards ranging from 0–12 μg bovine serum albumin (BSA) were prepared. The samples to be quantitated were prepared by diluted with dH_2O to within 5–20 μg/10 μl, 200 μl of the Bio-Rad protein assay reagent (Bio-Rad) was added to standards and each sample and mixed gently. After 10 min incubation, the absorbance (optical density value, OD) of the solutions was measured at 595 nm by using Perkin

Elmer UV/VIS Spectrometer Lambda 2, and the protein concentration of the samples calculated through linear regression plotting of the BSA standards.

3.5 Antibodies

Two anti-phospho-adducin (p-Add) antibodies were used. A rabbit polyclonal antibody from Santa Cruz Biotechnology (Santa Cruz, CA, USA) and a rabbit polyclonal antibody from Upstate Biotechnology (UBI, Lake Placid, NY, USA). The anti-p-Add antibodies (Santa Cruz and UBI) selectively recognize ser662 phosphorylated adducin γ, ser724 phosphorylated adducin α and ser713 phosphorylated adducin β. Two different polyclonal primary antibodies (goat anti-adducin α and rabbit anti-adducin β) were obtained from Santa Cruz Biotechnology (Santa Cruz, CA, USA), which against peptides mapping near the carboxy terminus of adducin α and β, respectively. Mouse monoclonal anti-microtubule associated protein-2 antibody (MAP-2, diluted 1:500) was from Chemicon International (Chemicon, Temecula, CA, USA). This antibody is directed to microtubules in neurons. In the central nervous system (CNS), MAP2 is confined to neuronal cell bodies and dendrites. Mouse monoclonal anti-SMI-31antibody (SMI-31, diluted 1:25,000) was obtained from Sternberger Monoclonals Incorporated (Sternberger, Lutherville. MD, USA). It is reacts with a phosphorylated epitope in phosphorylated neurofilament H (NF-H) and NF-M. Polyclonal rat anti-glial fibrillary acidic protein antibody (GFAP, diluted 1:200) was from EMD Biosciences (Calbiochem, San Diego, CA, USA). It is a marker for astrocytes. Appropriate secondary antibodies conjugated to FITC or Cy3 (Molecular Probes, Eugene, OR, USA) were used at a dilution of 1:100, or 1:600, respectively.

3.6 Western blot analysis

Protein samples were diluted with Laemmli sample buffer (BioRad, Hercules, CA, USA), boiled for 5 min then loaded and resolved on sodium dodecylsulphate-polyacrylamide gel electrophoresis (SDS-PAGE) gels (5% stacking gels and 8% separating gels). The gels were electrophoresed for 2.5 h at constant voltage between 50-100V.

After electrophoresis, the separating gels were transferred to polyvinylidene difluoride (PVDF, Bedford, MA, USA) membranes for 2 h at constant current of 200 mA. The membranes were blocked in 5% non-fat milk (w/v) and 0.025% NaN_3 in TBST-20 buffer (50 mM Tris base, 150 mM NaCl, 0.1% Tween-20 (v/v), pH 7.4). After blocking, membranes were rinsed with TBST-20 and incubated overnight at 4° C with anti-p-Add antibody (1:1000, UBI). The membranes were rinsed with TBST-20 followed by incubation with secondary antibodies for 1 h at room temperature.

The blots were developed with enhanced chemiluminescence reagent (ECL, Amersham, Piscataway, NJ, USA), and signals were captured by Scion Imaging software (NIH, Bethesda, MD, USA). All blots were normalized by probing for β-actin (Sigma, St. Louis, MO, USA). Results of normalized mean optical density values are expressed as mean ± SEM. Statistical comparison of p-Add expression level between wildtype and mSOD mice was evaluated by independent *t*-tests. Level of significance is $p < 0.05$.

3.7 Immunohistochemistry

For immunoperoxidase labeling, to abolish endogenous peroxidase activity, the free-floating sections were first incubated with 0.3% hydrogen peroxide in 10% methanol for 30 min. After blocking with 10% normal goat serum (NGS) in 0.3% Triton X-100 in 0.1 M PBS (PBST, pH 7.4) for 1 h, sections were incubated with primary antibodies to p-Add (1:000 for Santa Cruz; 1:200 for UBI) in PBST containing 10% NGS for 48 h at 4°C. Sections were then incubated with 1:500 biotinylated anti-rabbit secondary antibody (Vector, Burlingame, CA, USA) for 1 h at room temperature, followed by incubation with 1:1000 ABC reagent (Vector) in PBST for 90 min. Color development was performed using diaminobenzidine tetrahydrochloride (DAB) as a substrate for peroxidase and the reaction was stopped by flooding with dH_2O.

Immunofluorescence labeling was performed on floating sections after washing and blocking. Primary antibodies to p-Add were incubated for 48 h at 4°C at the 1:1000. After washing, donkey anti-rabbit secondary antibodies conjugated to Cy3 (Molecular Probes, Eugene, OR, USA) were used at a dilution of 1:600 in PBST containing 5% NGS for 1 h at room temperature. Sections were mounted onto slides, coversliped with Vectorshield (Vector, Burlingame, CA, USA).

For double immunostaining, primary antibodies were applied to the sections simultaneously. Appropriate controls were treated in an identical manner but without primary antibody and were evaluated in parallel.

Sections were examined using the Olympus BX40 microscope (Olympus America Inc., Melville, NY, USA). The filter sets for FITC and Cy3 are 470-490/515-550 nm (U-

MNIBA, Olympus America Inc., Melville, NY, USA) and 520-550/>580 nm (U-MWIG, Olympus America Inc., Melville, NY, USA), respectively. Images were acquired with a CoolSnap CCD camera (Photometrics, Tucson, AZ, USA) and MetaVue 4.6 software (Universal Imaging Corp., Downingtown, PA, USA).

3.8 Quantitative analysis of p-Add immunoreactivity

To quantify p-Add immunoreactivity in mSOD and wt mice, regions of interest (ROI) were defined morphologically in the central canal, ventral and dorsal horns of spinal cord. Four ROIs of identical size (60 x 60 pixels) were defined in each transverse section of spinal cord including both ventral and dorsal horns. To insure the uniformity of analysis, spinal cord sections were processed in parallel from both mSOD mice and littermate wt controls. The p-Add immunoreactivities in the ROIs were expressed as the mean pixel gray values from these ROIs. Measurements taken from the ventral horns or dorsal horns in each section were averaged to get one mean value for ventral and dorsal horn from each section. Data from five 50 μm thickness transverse sections obtained from the lower lumbar region (L3-5) of each animal were averaged for each data point. Densitometry was performed using NIH Image J software version 2.30 (NIH, Bethesda, MD, USA). Five sections per animal were believed to provide reliable mean density values for statistical analysis.

The ROI were defined to obtain consistent and unambiguous sampling regions. For calculating densitometry from the dorsal horn regions bilaterally, reference lines were drawn from the midpoint of the central canal to the dorsal horn region, at a 45 degree angle to the median plane. Points 75% of the length of this line away from the central point of the central canal were identified on both sides. Dorsal horn ROIs were used

where the ventro-lateral point of the square ROI (60 x 60 pixel) regions fell on the identified point. An analogous method was used to define ROIs for the ventral horn regions. To determine the p-Add immunoreactivity of the central canal, a circular ROI was drawn exclusively enclosing the central canal and not including the adjacent grey matter. Densitmometry for each of these regions was obtained using identical camera gains and settings using tissue processed in parallel. To correct for differences in background immunoreactivity, mean ROI values of tissue processed in parallel but without exposure to the primary antibody were subtracted from the ROI values that had been incubated with the corresponding primary antibody, for each of the animals used in the study. Statistical comparison of densitometric data between groups was evaluated by multivariate analysis employing a repeated measures general linear model or independent *t*-tests with groups defined as either mSOD or control for the individual ROIs examined. (Figure 3-1)

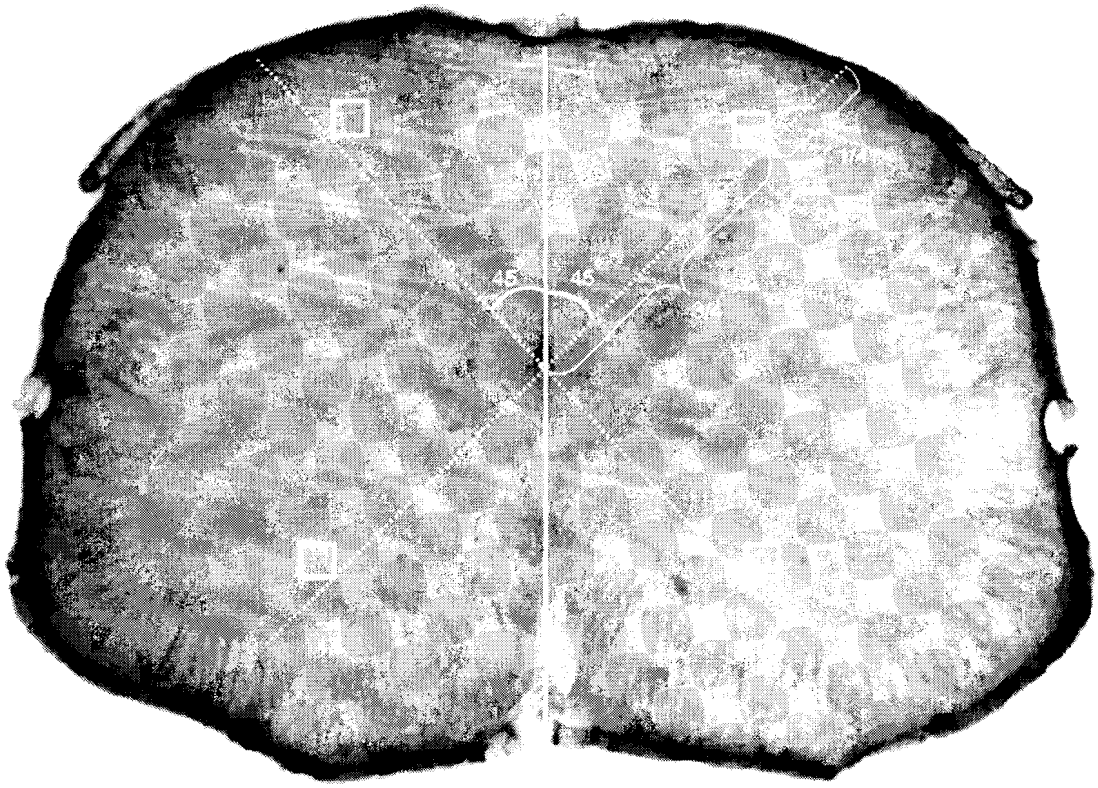

Figure 3-1: Quantification of p-Add immunoreactivity determined by sampling ROIs (60 x 60 pixels) in the regions of dorsal and ventral horns of spinal sections (open squares) and one ROI in the region of central canal (not shown). See Methods.

3.9 Confocal microscopy and imaging analysis

To compare the subcellular distribution of p-Add labeling in wild type and mSOD spinal cords, confocal images in the ventral horn were acquired using a Zeiss confocal microscope (X63 oil immersion lens) and LSM 510 (Zeiss, version 3.2), and images analysed using LSM Image Examiner software. This work has been done in collaboration with Dr. F. Cayabyab. Dr. Cayabyab was responsible for the actual image acquisition on the LSM. Both Dr. Cayabyab and I were responsible for image analysis.

To compare ventral horn motoneuron cellular morphologies, Z-stacked images (50-60 confocal slices of 0.5 μm thickness) of immunoreactive products of p-Add were projected in 3D on y-axis using the LSM 510 Image Examiner. Typically, I used conventional confocal microscopy to image spinal cords labeled with p-Add antibody. Cy3-conjugated secondary antibody was excited with a 543 HeNe laser and the emitted light filtered with a long pass 560 nm filter to visualize p-Add immunoreactive products. Images from spinal cords of end-point mSOD mice and wild type littermate controls were obtained and tissue was imaged using similar laser intensities and pinhole sizes.

To compare the relative intensities of plasma membrane and cytosolic p-Add labeling in wild type and mSOD ventral horn motoneurons, the average of five line intensity profiles was obtained using LSM Image Examiner for each motoneuron. The values of line intensity profiles were obtained by drawing straight lines originating just outside the plasma membrane boundary and extending to about 9 μm into the cytosol.

4 Results

4.1 Protein level of p-Add and adducin α and β in the spinal cords of mSOD mice

Western blotting of murine spinal cord tissue using p-Add antibodies demonstrated a protein band corresponding to 120kD (Figs. 4-1A and B). The position of this band is consistent with previous observations of p-Add immunoreactivity at the MARCKS-related domain in mammalian brain and spinal cord tissue (Matsuoka et al., 1998; Hu et al., 2003b). As shown on Fig 4-1A, Western blotting of p-Add did not reveal significant difference in protein level between control littermates and mSOD mice at pre-symptomatic stage (control; 0.81 ± .09; mSOD; 0.92 ± 0.11; mean ± SEM; n=4). At end stage (Figs. 4-1B), the mean value of level of p-Add in spinal cords of symptomatic mSOD mice was larger by 30%, compared to littermate controls, but this change was not statistically significant (control; 0.98 ± 0.24; mSOD; 1.30 ± 0.17; mean ± SEM; n=4). No significant differences were observed in the band densities of Western blots of spinal cord tissue for either α-adducin (Figs. 4-2A) (band at approx. 80 kDa; control; 0.64 ± .30; mSOD; 0.53 ± 0.09; n=4) or β-adducin (Figs. 4-2B) (band at approx. 80 KDa; control; 0.84 ± .14; mSOD; 1.07 ± 0.12; n=4).

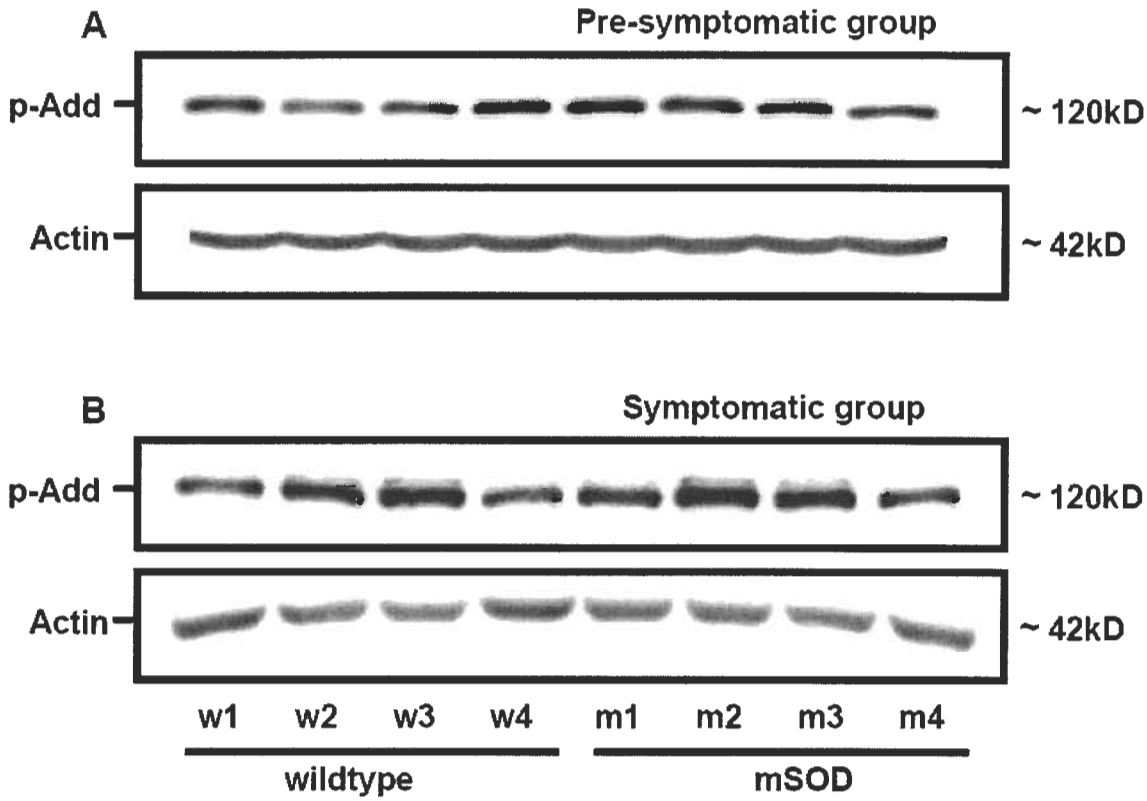

Figure 4-1: Protein level of p-Add by Western blot. A and B. No significant differences were found in the protein level of p-Add in spinal cord tissues from pre-symptomatic mSOD mice compared to littermate controls (A), or in mice at end-stage (B). Blots from affected animals and corresponding littermate controls are shown. Blots were normalized to actin.

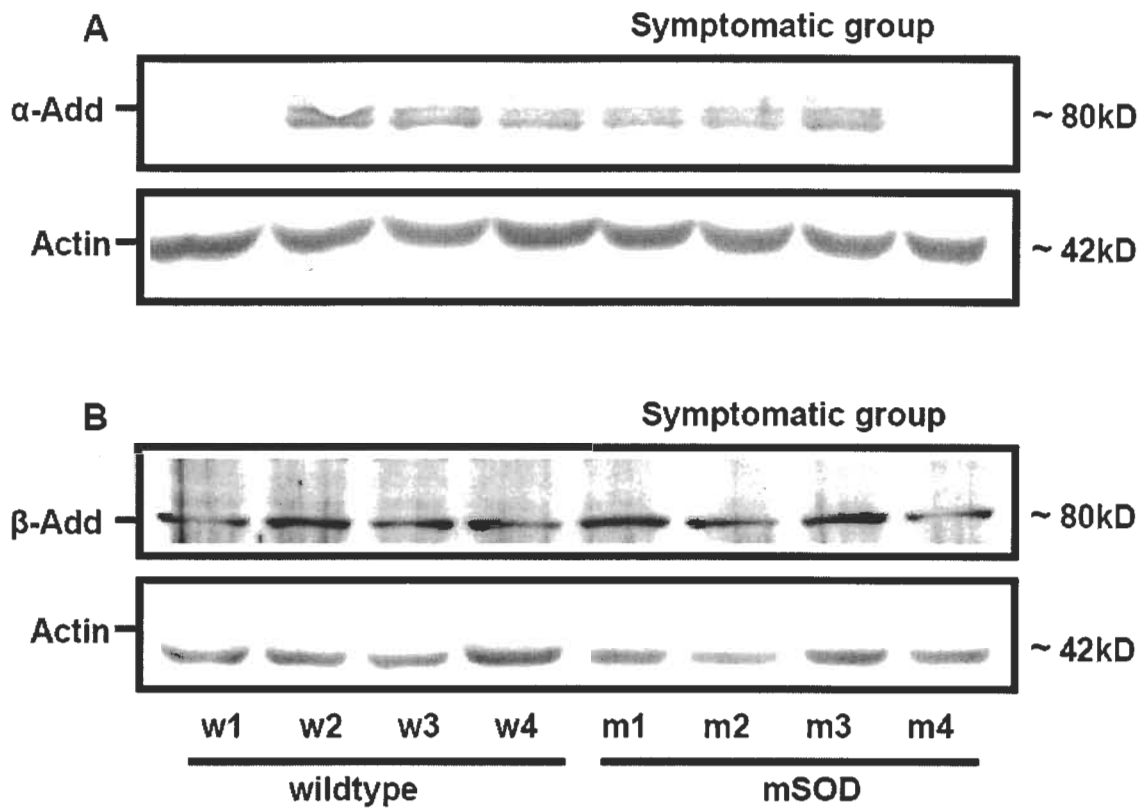

Figure 4-2: Protein levels of Adducin α (A) and Adducin β (B) by Western blot. No significant differences were found in the protein levels of Adducin α and β in spinal cord tissues from symptomatic mSOD mice compared to littermate controls. Blots were normalized to actin.

The immunoreactivity of p-Add has not previously been examined using immunocytochemistry in the mammalian spinal cord. To clarify the role of p-Add for motoneuron disease in the mSOD mouse and potentially in humans, we characterized the distribution of p-Add immunoreactivity in murine spinal cord.

4.2 Phospho-adducin immunoreactivity in the control mouse

4.2.1 General observation

The distribution of p-Add immunoreactivity in murine spinal cord is shown in Fig. 4-3A. Immunoreactivity against the MARCKS-related domain of p-Add is evident in several cell types within the spinal cord such as ventral horn neurons, glial fibers within the white matter and ependymal cells lining the central canal. Immunoreactivity to p-Add was evident in large cells of the ventral horn, both in the ventrolateral and ventromedial regions (Figs. 4-3A, 4-3B). These large, p-Add immunopositive cells were motoneurons as demonstrated by their position and by immunoreactivity for the neuron specific marker, MAP-2 (Figs. 4-3C, 4-3D and 4-3E). These p-Add+ neurons also demonstrated p-Add+, MAP-2+ dendrites, and axons projecting into the ventral white matter (Figs. 4-3F, 4-3G, 4-3H), confirming that they are motoneurons. In the transverse section of the lumbar region shown in Fig. 4-3A, p-Add immunoreactive motoneurons localize to the spinal nucleus of bulbocavernosus (SNB) medially, and the laterally situated, dorso-lateral nucleus (DLN) (Hamson et al., 2002). The extent of p-Add immunoreactivity of motoneurons was variable from section to section of thoracic and lumbar spinal cord. Generally, only a few motoneurons

demonstrated p-Add immunoreactivity in any given transverse section. For instance, in Figs. 4-3C and 4-3D, one motoneuron is seen expressing p-Add immunoreactivity and MAP-2 immunopositivity (Fig. 4-3D and 4-3E). Yet, other motoneurons and neurons adjacent to the p-Add immunoreactive cell do not demonstrate immunoreactivity against p-Add (Figs. 4-3D, 4-3G).

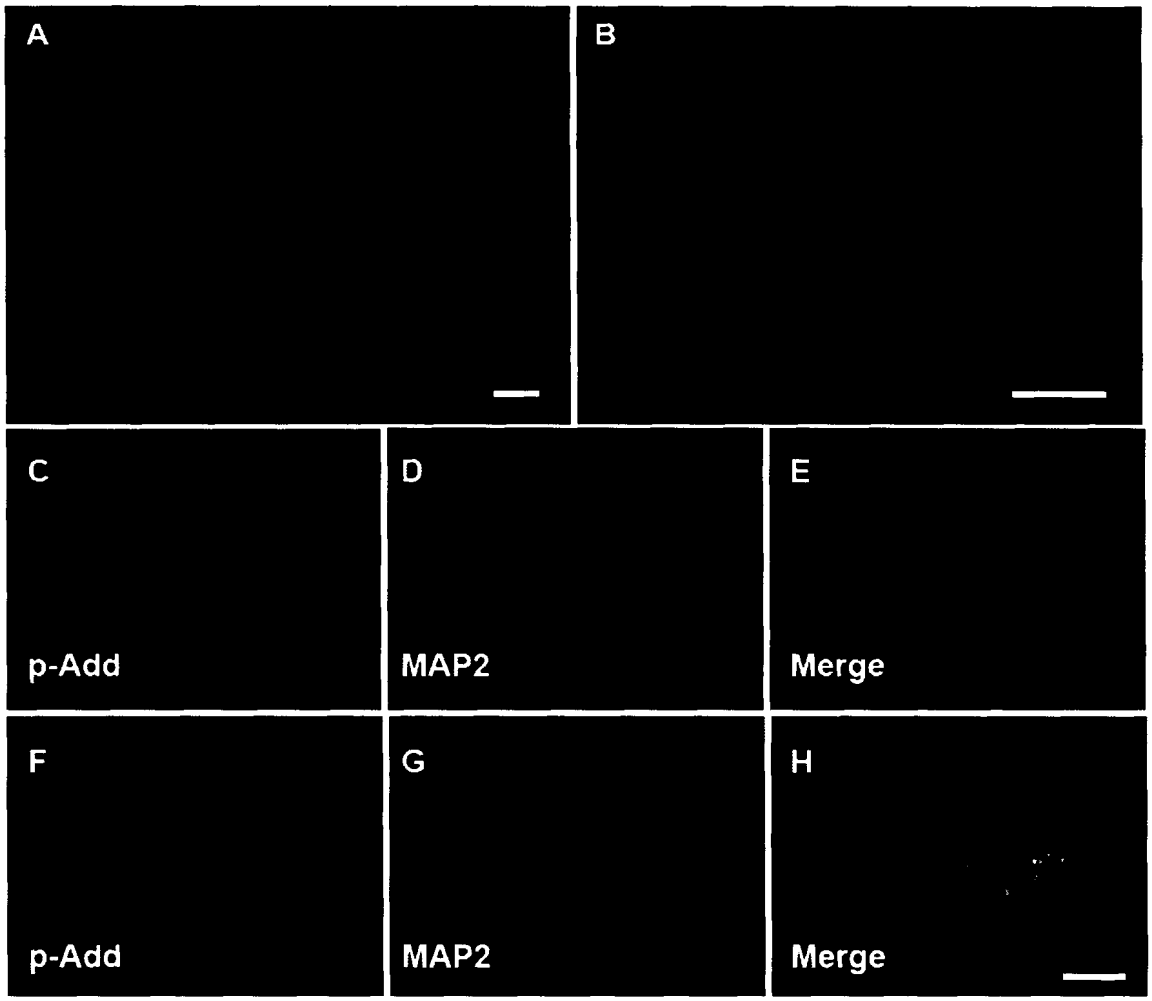

Figure 4-3: Immunoreactivity to p-Add is present in motoneurons, ependyma and white matter. *A and B,* Sections of wild type mouse labeled for p-Add, *B* is magnified region of *A*. *C-H,* sections double labeled for p-Add (*red*; *C,F*) and MAP-2, a neuronal marker (*green*; *D,G*), co-localization as demonstrated by yellow color in *E, H.* Scale bars: *A,* 100μm; *B-H,* 50 μm.

4.2.2 Central canal, white matter and dorsal horn

As shown in Figs. 4-3A, 4-4A and 4-4B, p-Add immunoreactivity is evident in ependymal cells of the central canal. More specifically, p-Add immunoreactivity is most evident over the basal surfaces of ependymal cells, but is also present over the lateral cytoplasmic surfaces of these cells. Extending from the basal aspect of the ependyma was dense p-Add immunopositive fibres that radiated tangentially from the central canal. Most frequently, these fibers ran dorso-ventrally along the midline. Several individual p-Add+ fibers would sometimes run in parallel. Other p-Add immunoreactive fibers ran laterally, often for considerable distances (Fig. 4-4A). Immunostaining for p-Add was also seen in radially organized fibers in the white matter over the ventral, lateral and dorsal aspects of the spinal cord (Figs. 4-4A and 4-4C). These radially organized fibers are shown in the ventral white matter in Fig. 4-4C where they course towards the pial surface. From the shafts of these fibers project short, laterally-protruding 'side arms'. These p-Add-expressing fibers also demonstrate immunoreactivity to GFAP (Figs. 4-4D and 4-4E) indicating that some, but not all of these p-Add+ fibers are astrocytes. The extensive length of these astrocytes, their orientation perpendicular to the surface of the spinal cord and their position close to the pial surface also suggests that they are radial glia (McMahon and McDermott, 2002). Additional pAdd+ fibers observed within the ventral white matter included the axons of motoneurons (Fig. 4-4F, and below).

Figure 4-4F shows a low power view of murine spinal cord demonstrating prominent immunoreactivity for p-Add over the superficial aspects of the dorsal horns. To clarify the cell types that demonstrated p-Add immunoreactivity we used double labeling with GFAP as well as p-Add. As shown in Figs. 4-4G and H, GFAP

immunoreactive astrocytes were seen that also demonstrated p-Add immunoreactivity. Other GFAP cells did not show p-Add immunopositivity indicating that many, but not all of the p-Add fibers and cells in the dorsal grey matter were astrocytes.

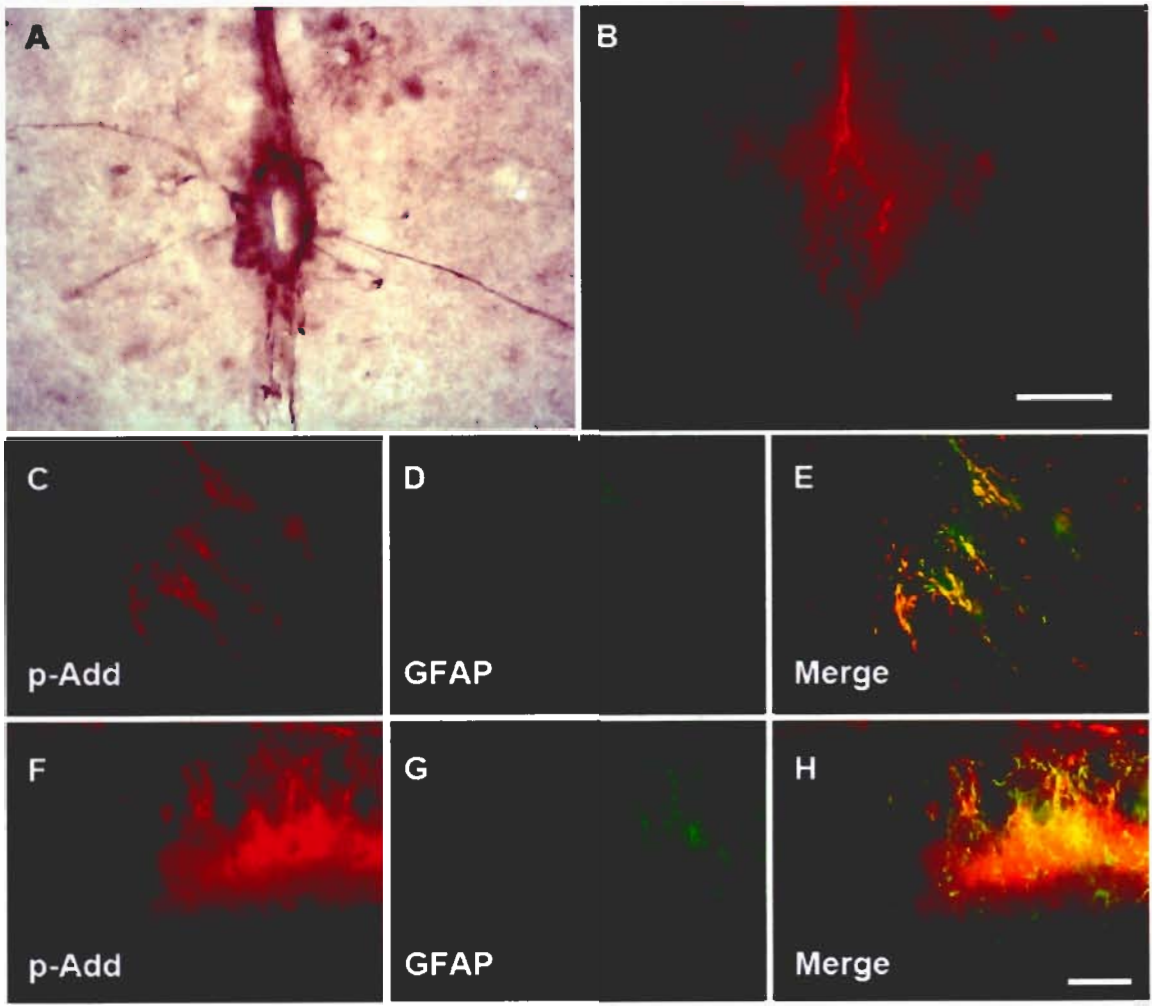

Figure 4-4: Immunoreactivity to p-Add in ependyma and astrocytes. *A and B*, sections from wild type mice labeled with p-Add reveal immunostaining of ependyma using DAB and Cy3, respectively. *C-H*, sections double labeled for p-Add (*red*; *C, F*) and GFAP, an astrocyte marker (*green*; *D, G*), co-localization in the region of ventral white matter (*C, D* and *E*) and dorsal horn (*F, G* and *H*) as demonstrated by yellow color in *E, H*. Scale bars: 50 μm.

4.3 Phospho-adducin immunoreactivity in the mSOD mouse

We expected to see differences in the pattern of p-Add immunoreactivity in spinal cord sections between disease and control mice. Fig. 4-5 shows the expression of p-Add immunoreactivity in lumbar spinal cord sections from wt (A,C,E,G) and mSOD mice (B,D,F,H) using identical reaction conditions for Figs. 4-5A-D and 4-5E-H. In control mice, p-Add immunolabeling was largely confined to the central canal and superficial dorsal horn (Figs 4-5A, E). In contrast, spinal cord tissue from mSOD mice demonstrated prominent p-Add immunoreactivity in the ventral horns and intermediate zones of grey matter in addition to slightly increased p-Add immunoreactivity in the superficial dorsal horn region (Figs 4-5B, F). The p-Add immunoreactivity in mSOD mice was easily detected at low power magnification where the transition between p-Add immunoreactive grey matter and background, non-immunoreactive tissue was relatively abrupt (Fig. 4-5B). Figs. 4-5C and 4-5D demonstrate the much higher p-Add immunoreactivity seen in the ventral horns of the mSOD mice (D), compared to wt littermates (C). Similar findings were observed using immunofluorescence labeling for p-Add (Figs 4-5E and F). Using immunofluorescence, only limited p-Add immunoreactivity was seen in spinal cord sections from wt mice (4-5E). This immunoreactivity was primarily localized to the central canal and the dorsal horn. In mSOD mice, extensive p-Add immunoreactivity was observed throughout the ventral and intermediate zones, extending even into the dorsal horns (4-5F).

Figure 4-5: Distribution of p-Add immunoreactivity in wild type and mSOD mice. Lumbar sections from wild type (left panels) and mSOD mice (right panels) immunolabeled with p-Add antibody. For DAB staining, *A* is lumbar section of wild type and *B* is mSOD spinal cord; *C* and *D* are magnified regions of ventral horn from *A* and *B*, respectively. For immunoreactivity for p-Add visualized by Cy3, *E* is from wild type and *F* from mSOD; *G* and *H* are magnified regions of ventral horn from *E* and *F*, respectively. Scale bars: *A, B, E and F*, 100μm; *C, D, G and H*, 50 μm.

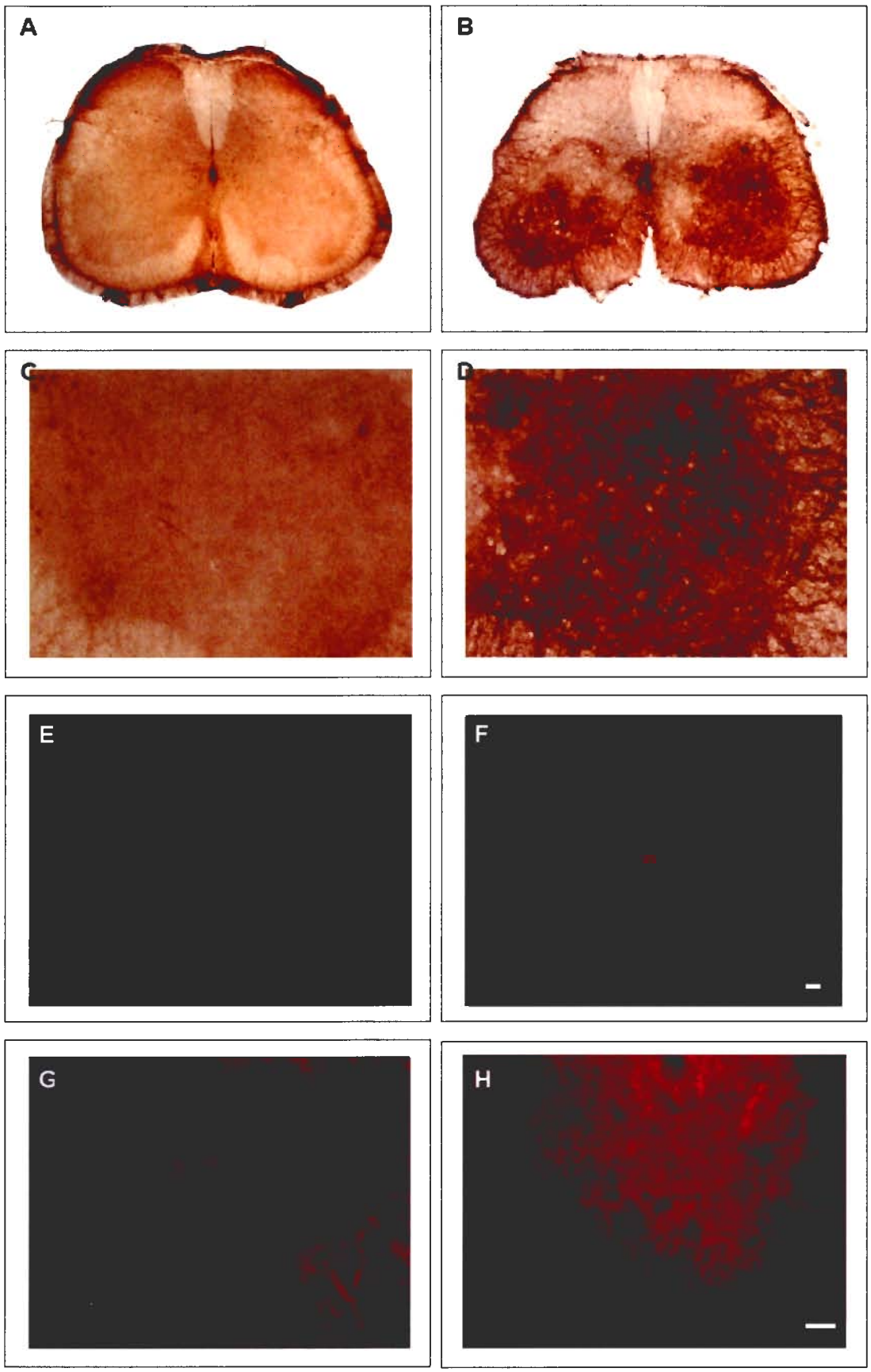
A
B
C
D
E
F
G
H

To quantify differences in p-Add immunoreactivity in mSOD and control mice, we measured the relative amounts of p-Add immunoreactivity in the dorsal horns, ventral horns and central canal, using densitometry of defined regions of interest, as described above (see methods; Fig. 3-1). Using relative densitometry, we found that in control mice, mean p-Add immunoreactivity was significantly greater in the central canal (148.2 $\pm$ 14.4 units; mean $\pm$ SEM; $p < 0.01$) compared to p-Add immunoreactivity in either ventral (32.1 $\pm$ 6.0) or dorsal horn (17.4 $\pm$ 3.7; Fig 4-6). Mean p-Add immunoreactivity was significantly greater in both the dorsal (50.0 $\pm$ 12.5, $p < 0.05$) and ventral horns (108.1 $\pm$ 10.2, $p < 0.01$) of mSOD mice, compared to wild type littermate controls, but no significant difference in immunoreactivity was evident in central canal regions (133.2 $\pm$ 7.0; Fig 4-6). The increase in p-Add immunoreactivity in mSOD mice was evident in the grey matter and was confluent within this region.

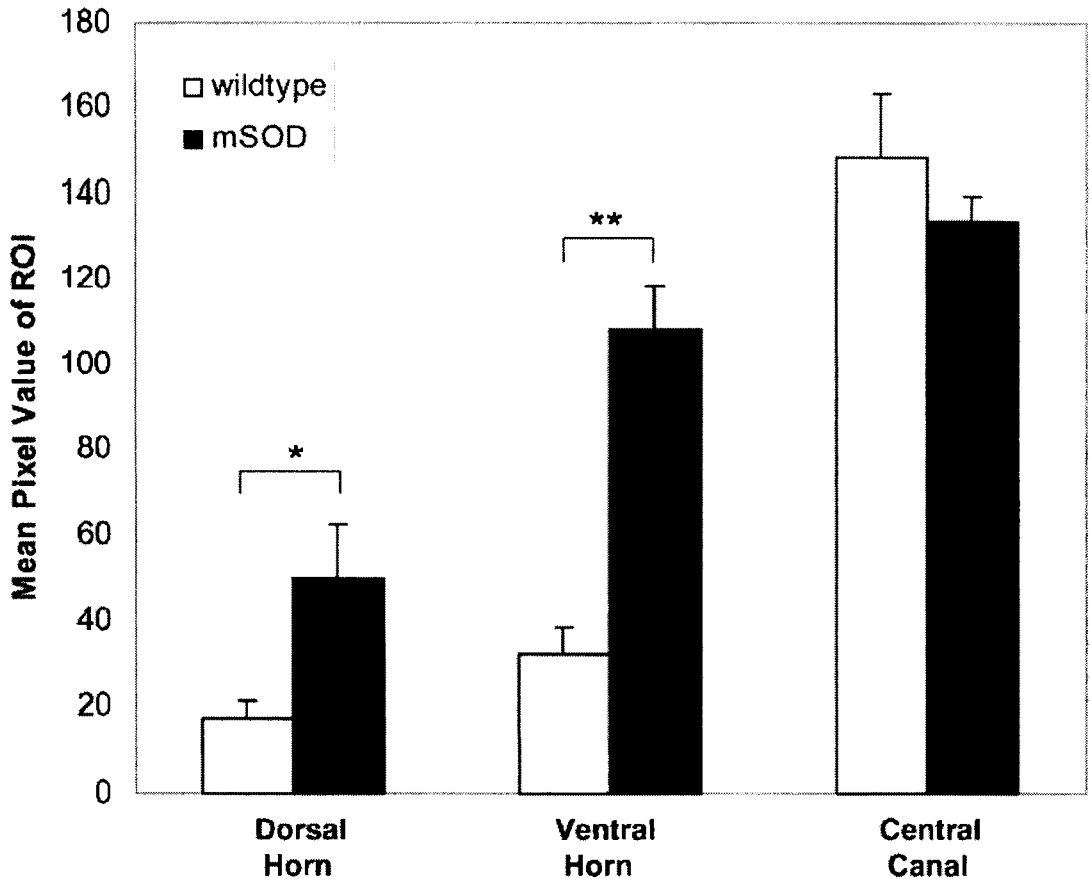

Figure 4-6: Relative quantification of p-Add immunoreactivity in lumbar spinal cords (mSOD n = 5, wild type n = 5). Overall effects were evaluated by multivariate analysis employing a repeated measures general linear model. Comparison between two groups were performed by independent t-tests, *P < 0.05, ** P < 0.01, respectively. P-Add immunoreactivity is increased significantly in both the ventral and the dorsal horn regions of mSOD mice compared to wild type littermate controls.

Examination of the ventral horns and adjacent ventral white matter revealed that in mSOD mice motoneuron axons exhibited extensive vacuolation, as has been reported previously (Chiu et al., 1995). These dilated and vacuolated axons revealed clear p-Add immunoreactivity, especially in dilated axonal segments lying within the ventral grey and ventral white matter (Fig. 4-7B). These vacuoles were never seen in motoneuron axons of wt mice (Fig. 4-7A). The numerous vacuoles present in some motoneuron axons produced a 'beaded appearance' of the axon. Some of these axonal vacuoles that exhibited pAdd immunoreactivity were also labeled with antibodies to neurofilament (SMI31; Figs. 4-7C, 4-7D, 4-7E).

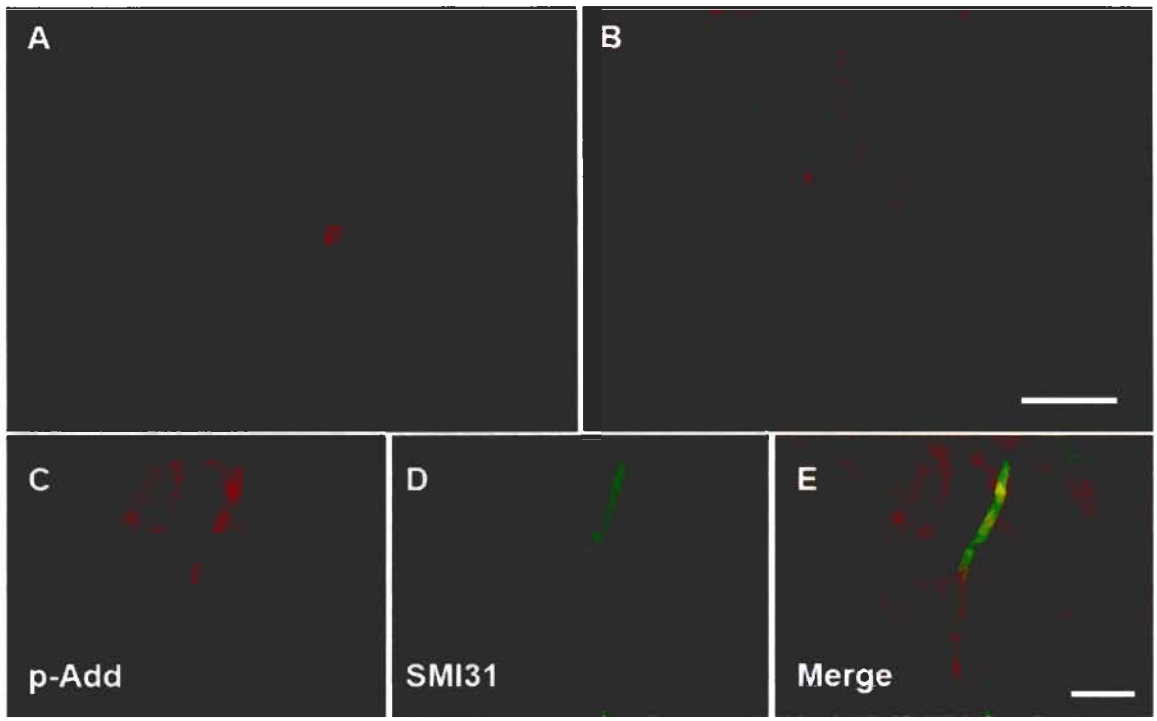

Figure 4-7: Immunoreactivity to p-Add in motoneuron axons. *A* and *B,* sections of wild type and mSOD mice labeled with p-Add. *C, D* and *E*, sections from mSOD mouse double labeled for p-Add (*red*; *C*) and SMI31, a marker for neurofilament (*green*; *D*), co-localization as demonstrated by yellow color in *E*. Scale bars: 50 μm.

4.4 Increased p-Add immunoreactivity in mSOD mice localizes to astrocytes

To determine which cell types manifest the increase in p-Add immunoreactivity in spinal cords of mSOD mice I evaluated spinal cord tissue using markers of neurons and non-neuronal cells. As shown in Fig. 4-8, spinal cord sections from mSOD mice exhibit a considerable increase in GFAP immunoreactivity, as has been demonstrated previously (Hall et al., 1998). We observe that the increase in p-Add immunoreactivity in mSOD mice localizes to the regions of increased GFAP immunoreactivity (Figs 4-8D, 4-8E, 4-8F), compared to control (Figs 4-8A, 4-8B, 4-8C), indicating that some of the increase in p-Add immunoreactivity is due to increased glial expression of p-Add.

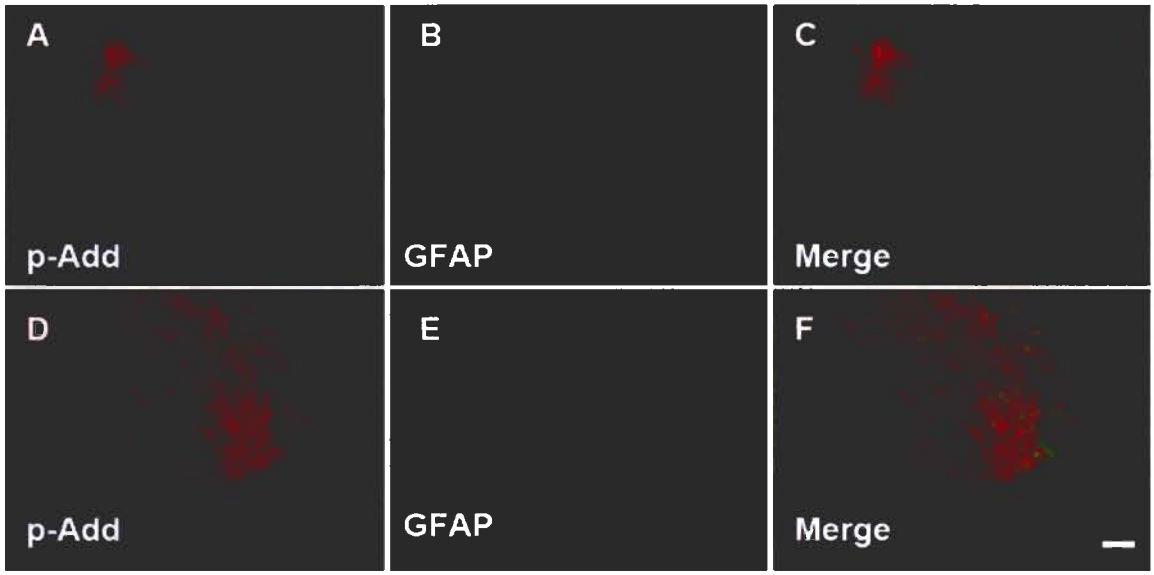

Figure 4-8: The increase in p-Add immunoreactivity in mSOD mice localizes to the regions of increased GFAP immunoreactivity. *A, B* and *C* are sections from wild type mice; *D, E* and *F* are from mSOD mice. Sections were double labelled for p-Add (*red*; *A, D*) and GFAP, a marker for astrocytes (*green*; *B, E*), showed colocalization in the region of ventral horn (*C, F*) as demonstrated by *yellow*. Scale bars: 100 μm.

4.5 Subcellular locolization of p-Add in motoneurons

To further examine the cellular and subcellular distribution of p-Add near the central canal of spinal cords of wild type and mSOD mice, *Z*-stacked images were acquired using confocal microscopy and projected in 3D on the y-axis. Similar to results shown with conventional epifluorescence microscopy (Fig. 4-3A, 4-3B), p-Add immunoreactivity was present in ependyma lining the central canal in both mSOD and age-matched wild type spinal cords (Figure 4-9A, 4-9C). In single confocal slices acquired near the middle of the tissue sample, the p-Add immunoreactivity decorated the plasma membrane of ependymal cells (Fig. 4-9B, 4-9D). Fibers running dorso-ventrally as well as medio-laterally were labeled with p-Add and were prominently expressed both in mSOD and in wild type spinal cords.

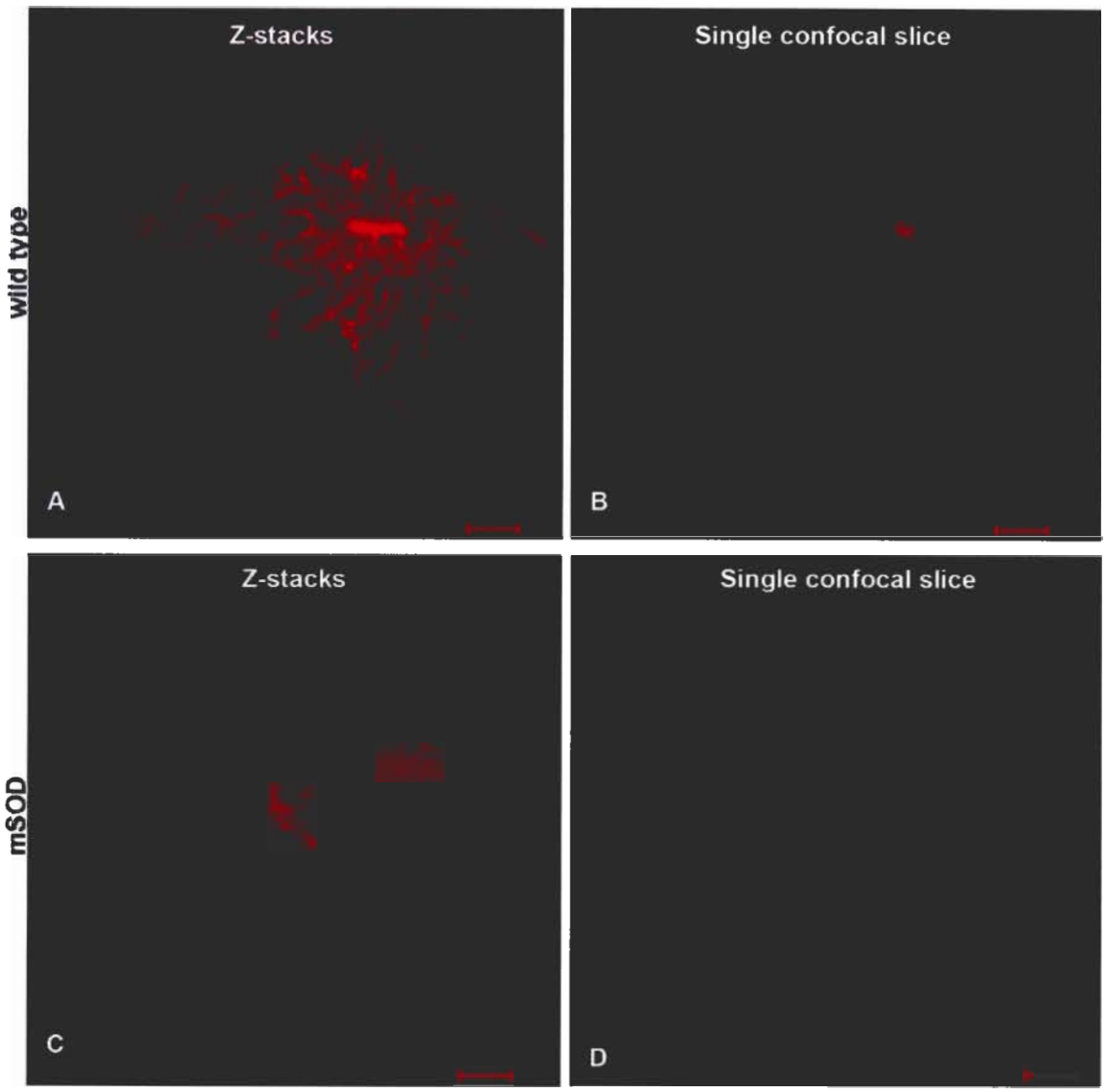

Figure 4-9: Confocal images of the central canal of wild type and mSOD spinal cords. *A, C,* Z-stacked images of the central canal were used to reconstruct the 3D images projected on the y-axis. *B, D,* Single confocal images of the central canal showing expression of pAdd-immunoreactive products in the plasma membranes of ependyma. Spinal cords were labeled with p-Add primary and Cy3-conjugated secondary antibodies. Scale bars: 20 μm.

Using confocal microscopy, I found that ventral horn motoneurons (previously identified by their size and shape and by their immunoreactivity to MAP-2 antibody) expressed higher levels of pAdd immunoreactivity in mSOD compared to age-matched littermate control mice (Figure 10). A few p-Add-immunoreactive ventral horn motoneurons were often surrounded by other weakly labeled motoneurons, as shown in the 3D reconstruction of the Z-stacked images (Figure 4-10A). Some motoneuron somas of wild type spinal cords appeared to show punctate staining localized in the cytosol near the perinuclear regions, as shown in single confocal slices (Figure 4-10B). In contrast, the 3D reconstructed images of the mSOD spinal cords shows higher intensity of p-Add resulting from p-Add-immunoreactive motoneuron somas as well as other smaller somas and processes (likely from astrocytes) (Figure 4-10C). In single confocal slices, the mSOD motoneurons appeared to have less intracellular perinuclear punctate staining (Figure 4-10D vs. 4-10B). A redistribution of the p-Add immunoreactivity of motoneurons from the cytosol to the subplasma-membrane domains appears to accompany the phosphorylation changes in mSOD mice. The p-Add immunoreactivity was increased near the plasma membranes of mSOD motoneurons compared to controls (Figures 4-10D vs. 4-10B; and summarized in Figure 4-11).

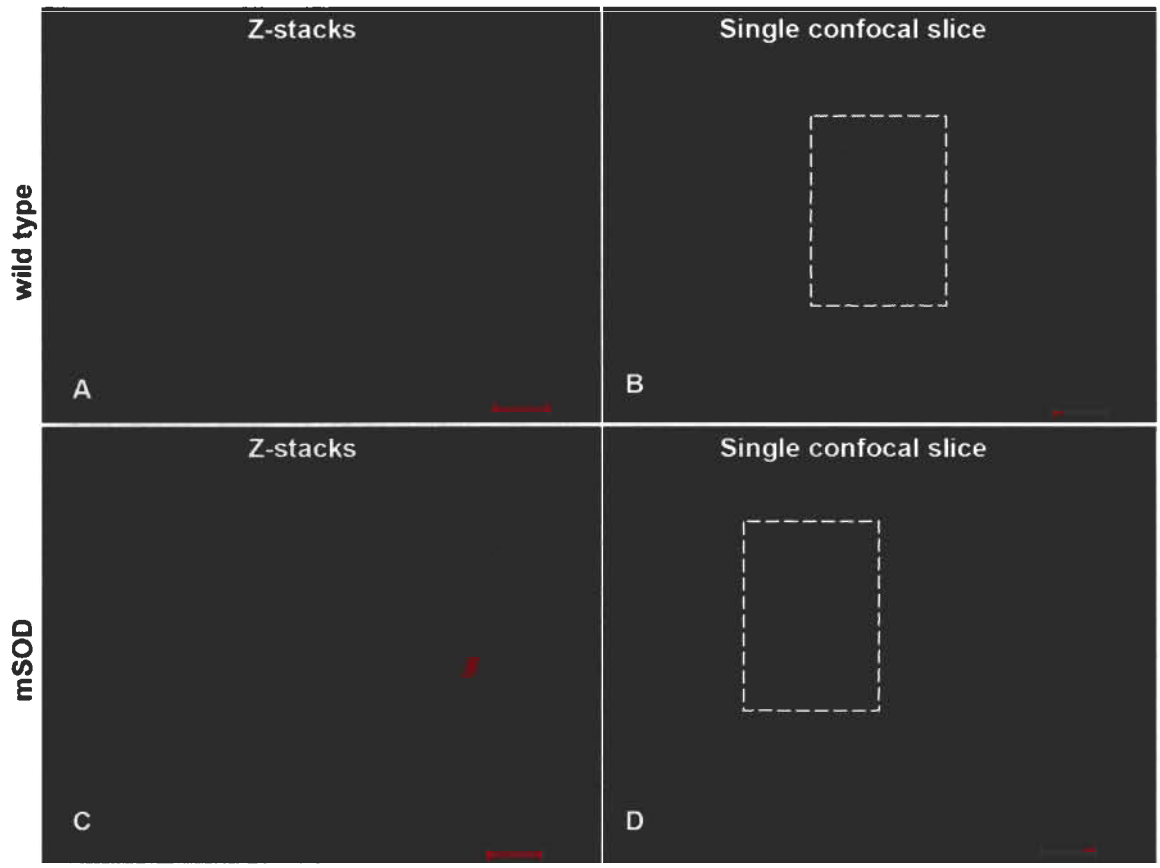

Figure 4-10: Confocal images of wild type and mSOD motoneurons. The 3D reconstructed images (projected in the y-axis, *A* and *C*) shows more p-Add labeling in mSOD spinal cords. Single confocal images (*B* and *D*) show greater sub-plasma membrane staining of p-Add in mSOD. Scale bars: 20 μm.

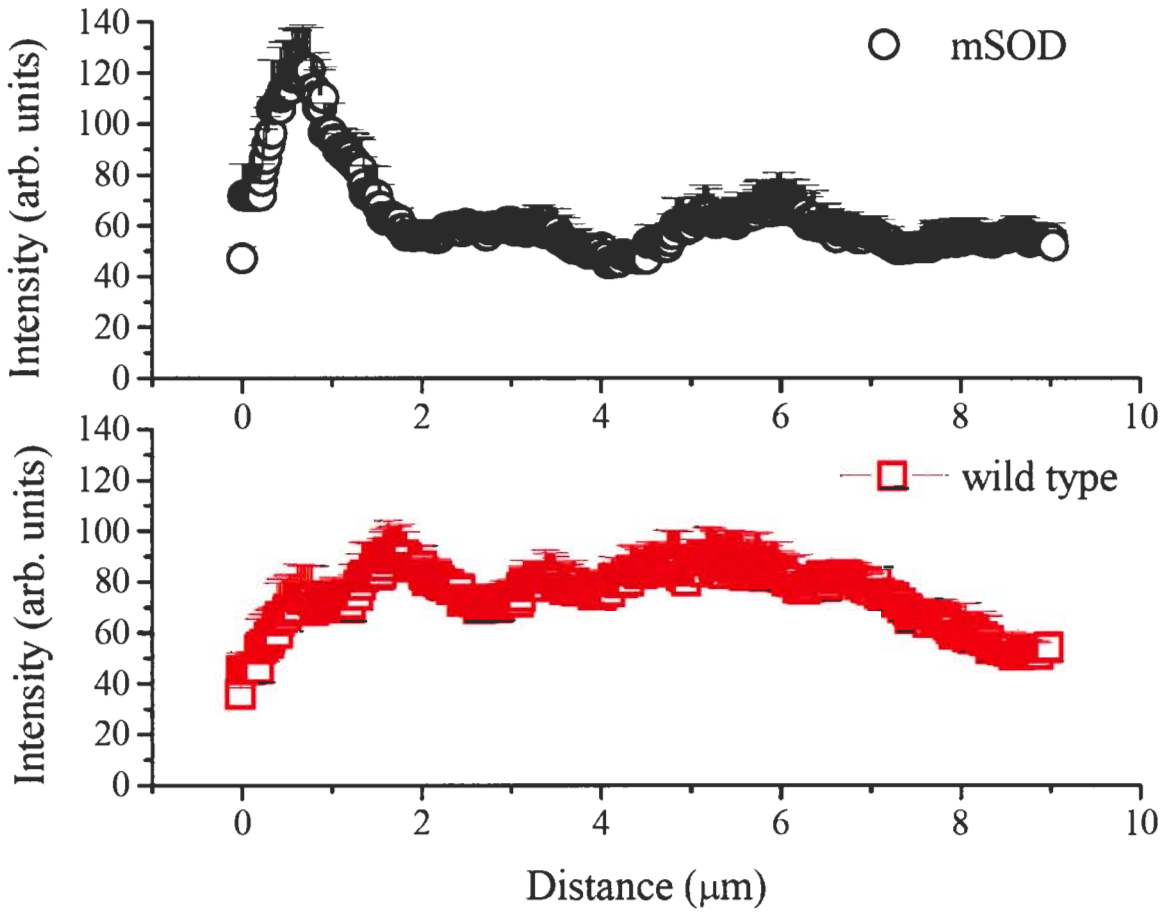

Figure 4-11: The relative intensities of plasma membrane and cytosolic p-Add labeling in wild type and mSOD ventral horn motoneurons by obtaining line intensity profiles using LSM Image Examiner for each motoneuron. Again, it is showed that greater sub-plasma membrane staining of p-Add in mSOD compared to wild type mice (corresponding to the boxed motoneurons in Figure 10*B* and 10*D*, see Methods for details).

In other experiments using two-photon laser scanning microscopy (TPLSM), spinal cords from other symptomatic and age-matched control animals revealed more punctate p-Add immunostaining in the cytosol of wild type motoneurons, but these punctate reactive products were not associated with the sub-plasmalemmal membrane (Figure 12A). In contrast, in age-matched mSOD spinal cords, some motoneuron somas showed fewer and less intense cytosolic immunoreactive products, but some punctate p-Add immunoreactivity localized near the subplasmalemma (Figure 12B). Often there are highly stained fibers and processes present surrounding the motoneuron somas of mSOD mice (Figure 10B and Figure 10D).

Figure 4-12: Two photon laser scanning microscopy (TPLSM) images of wild type and mSOD motoneurons and subcellular localization of p-Add immunoreactivity. *A,* Wild type motoneurons show polarized cytosolic localization of small (0.5-2 μm) puncta immunoreactive to the p-Add antibody. *B,* Ventral horn motoneurons of mSOD mice show less punctate immunoreactive products near perinuclear regions than controls, and some motoneurons show dispersed puncta and migration of p-Add immunoreactive products to sub-plasmalemmal domains. Spinal cords were labeled with p-Add. Scale bars: 20 μm.

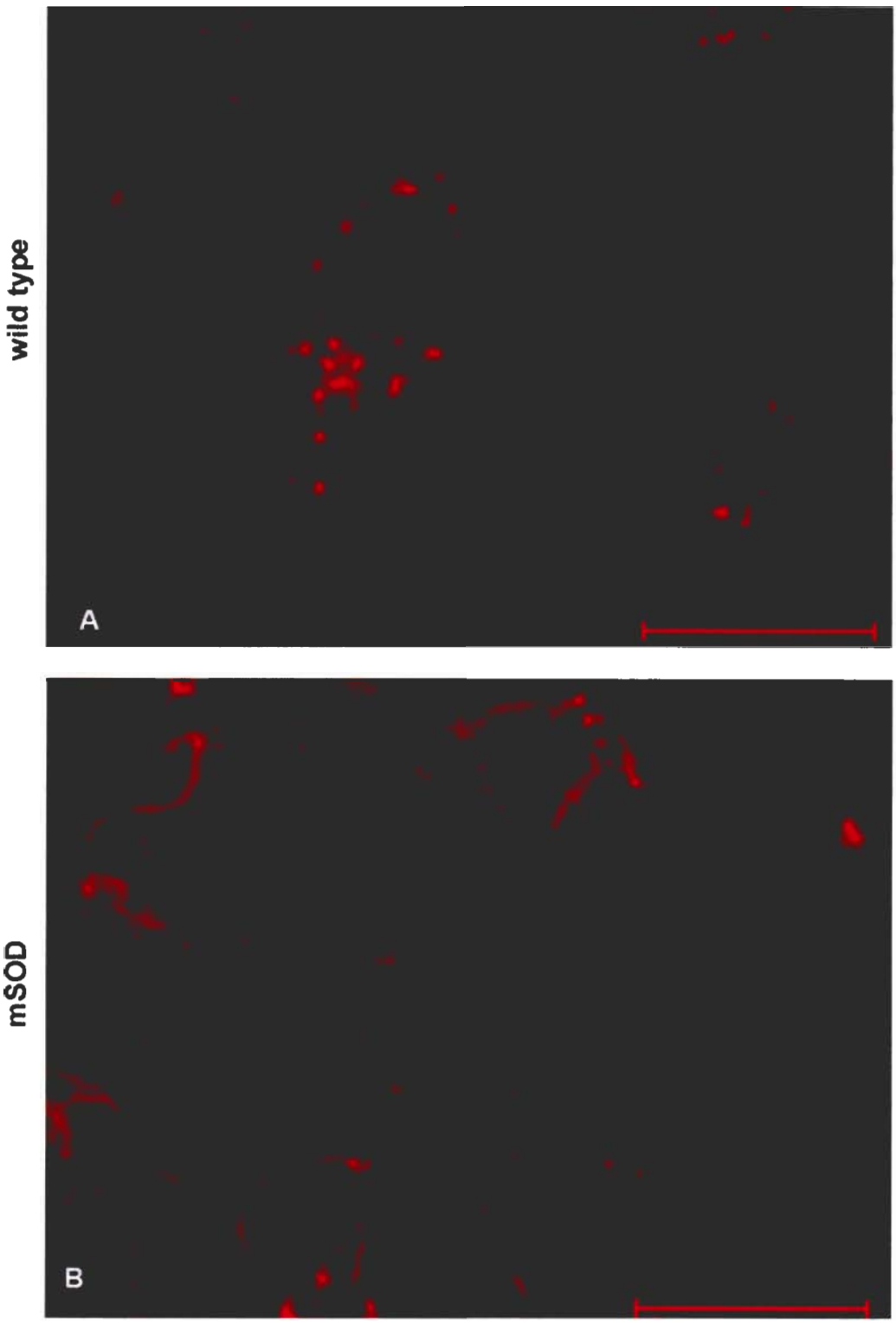
wild type
A
mSOD
B

5 Discussion

There is considerable interest in identifying proteins that might be responsible for the selective vulnerability of certain populations of neurons to disease. For instance, the presence of excitatory amino acid receptors and associated ligand-gated channels permit the death of neurons expressing these receptors following exposure to an appropriate ligand. It is also possible that the expression of certain structural proteins may also be relevant for the selective vulnerability of specific neuron populations. One group of structural proteins that are of particular interest is the adducins. The adducins are a family of proteins that are involved in the assembly and disassembly of actin and spectrin filaments at the plasma membrane. This group of structural proteins is located predominantly is membrane regions highly enriched with synapses, suggesting that adducins are associated with neurotransmitter receptors (Matsuoka et al., 1998).

In previous observations using a multi-immunoblotting analysis, Hu et al. (2003b) found significant elevations in protein levels of p-Add in cytosolic fractions of spinal cord tissue from ALS patients, compared to controls. Hu et al. also previously reported significantly increased protein level and activation of PKC isoforms in spinal cord tissue from ALS patients compared to controls (Lanius et al., 1995; Hu et al., 2003b). As PKC, but not PKA, phosphorylates adducin at the MARCKS-related domain recognized by the p-Add antibodies used here (Matsuoka et al., 1998), these data suggest that one action of

the elevated PKC activity in ALS tissue is the phosphorylation of adducin, which could play some role in the disease process.

In the present work I wished to determine the protein level and localization of p-Add in the mammalian nervous system, as there is only a single report on this subject which is confined to p-Add localization in the hippocampus (Matsuoka et al., 1998). The distribution of adducin or p-Add has not been previously determined in mammalian spinal cord.

I found p-Add protein was detected in murine spinal cord as an approximately 120 kD band on Western blots. This is consistent with previous findings in rat hippocampal tissue (Matsuoka et al., 1998). In Western blots of human spinal cord tissue we found previously that these same p-Add antibodies labeled two bands, the upper band at approx. 120 kD likely reflecting phosphorylation of α-adducin at ser724 and a lower band was seen at approx. 80 kD and likely is generated by the phosphorylation of γ-adducin at ser662 (Hu et al., 2003b). In these studies p-Add protein in control human spinal cord tissue was not prominent. However, tissue from patients who died with ALS had highly significant increased protein level of p-Add, both at 120 and 80 kD, and from both the cytosolic and membrane-associated tissue fractions (Hu et al., 2003b). The protein corresponding to the 120 kD band in mSOD mice, compared to controls, using the p-Add antibodies used here is consistent with increased phosphorylation at the MARCKS-related domain of α, β, and /or γ adducin. I did not observe any bands at 80 kD in Western blots of murine spinal cord tissue in the present study suggesting that the p-Add expression in spinal cord is derived from ser724 of α-adducin, or less likely

ser713 of β-adducin, and not from the phosphorylation of ser662 of γ-adducin, and likely due to species differences.

5.1 Distribution of p-Add in control spinal cord

The observation of altered protein level of p-Add in ALS patients prompted us to explore the distribution of p-Add in spinal cord tissue. The immunoreactivity of p-Add has not previously been examined using immunocytochemistry in the mammalian spinal cord. In murine spinal cord, p-Add had a remarkably consistent immunocytochemical distribution. Prominent p-Add immunoreactivity was evident in the central canal, where ependymal cells were labeled with p-Add, especially in the vicinity of the basal and lateral membranes. A number of p-Add immunoreactive fibers radiated from the ependymal cells of the central canal. These fine fibers were GFAP- and SMI-31- and their identity is unclear. However, they had a resemblance to radial glial fibers, which can be GFAP- in adult mice (Rakic, 2003). The p-Add expression of these fibers did not appear to differ in wt and mSOD mice, and their identity was not pursued further in this study. Cells of the dorsal horn were also labeled with antibodies to p-Add and some of these cells were GFAP+. In addition, many fibers in the white matter were p-Add+ and GFAP+ consistent with evidence that p-Add is expressed by astrocytes. Previous data has shown that α-adducin is expressed in glial cells (Seidel et al., 1995). Immunoreactivity of p-Add was also observed on the somata, dendrites and axons of motoneurons.

5.2 Phospho-adducin immunoreactivity in symptomatic mSOD mice

Mice that over-express mSOD (G93A; line G1H) by 10-20 folds remain clinically asymptomatic until around 100 days of age when they manifest hind limb weakness that results in a slow, unstable gait (Gurney *et al.*, 1994). By day 120-125 many are unable to right themselves and have difficulty feeding (Gurney *et al.*, 1994; Hamson *et al.*, 2002). These G93A mice are a good model of ALS; the mSOD mutation is detected in patients with FALS and the specific mSOD mutation in these mice correlates with disease onset and the rate of progression, as in ALS (Gurney *et al.*, 1994). Generally, an reduction of motoneuron numbers by 40-60% are seen in mSOD mice at 'end-stage' (Mohajeri et al., 1998; Hamson et al., 2002). These reductions in motoneuron number are similar to the extent of motoneuron loss in ALS patients at autopsy (Tsukagoshi *et al.*, 1979). Western blotting of p-Add did not reveal significant differences of p-Add protein content in mSOD mice, compared to littermates, either at pre-symptomatic or at end-stage.

Regional analysis of p-Add immunoreactivity demonstrated that ventral horn and to a lesser extent dorsal horn of spinal cord have increased p-Add immunoreactivity that localizes to some motoneurons as well as astrocytes. Likely, this regional increased p-Add immunoreactivity pattern in mSOD mice is not sufficiently widespread to produce a significant increase in p-Add protein level by Western blotting. It is not known whether the increase in p-Add has functional implications. As p-Add is phosphorylated on the MARCKS domain by PKC, it seems likely that the increase in p-Add content in mSOD mice could be secondary to increased PKC phosphorylation, which is likely present in spinal cord tissue from patients with ALS (Hu et al., 2003b). Against this possibility is the observation that the protein levels of several PKC isoforms are not different in mSOD

mice compared to controls, as determined by a multi-immunoblotting technique (Hu et al., 2003a). However, the sensitivity of the multi-immunoblot technique may be insufficient to detect a difference in PKC content between mSOD and wt mice. The activities of PKC in mSOD mice have not been determined.

5.3 Elevated phosphoprotein immunoreactivity in mSOD mice and in ALS

These data demonstrate that p-Add immunoreactivity is higher mainly in the ventral horn regions of lumbosacral spinal cord from mSOD mice than in wt controls. Increased immunoreactivity of p-Add is a further addition to a list of phosphoproteins that are over-expressed in mSOD mice compared to wt littermates and in nervous system tissue from ALS patients, compared to controls. For instance, in a recent study we found elevated protein level and/or activation of many protein kinases in ALS tissue (Hu et al., 2003b). These protein kinases included PKCα, PKCβ, PKCζ and GSK3α/β, which might augment neural death in ALS, and CaMKK, PKBα, Rsk1, S6K, and SAPK, which may be a response to neuronal injury that potentially can mitigate cell death. Furthermore, aberrant hyperphosphorylation of the microtubule-associated protein, tau, has been found both in a mouse model of ALS over-expressing human mutant SOD (G37R; Farah et al., 2003), and in frontal cortex tissue from patients who died from ALS, especially those that manifested cognitive impairment (Yang et al., 2003). The hyperphosphorylation of tau may be linked to increased protein level of Cdk-5, which has also been reported in mSOD over-expressing mice (Nguyen et al., 2001). Additionally, p38α, a member of the stress-activated protein kinase family, has been found to be associated with the abnormally phosphorylated side arms of neurofilament heavy and neurofilament middle proteins in

ALS tissue, as well as in mice over-expressing human mutant SOD (Ackerley et al., 2004).

The presence of increased content of a number of phosphoproteins in mSOD mice raises the possibility that up-regulation of phosphorylation is a more general feature of this neurological disorder (Krieger et al., 2003). However, it is not clear if this increase in phosphorylation activity is a consequence of neuronal destruction, or reflects the action of regenerative mechanisms.

Wagey et al (1997) have previously proposed that the finding of hyperphosphorylation of a number of phosphoproteins in ALS tissue could be the result of impaired activation of one or more protein phosphatases. Protein phosphatases are responsible for the de-phosphorylation of protein kinases or phosphoproteins. Although the previously reported findings were consistent with this hypothesis (Wagey et al., 1997), more recent observations have not demonstrated impairments in the activation and content of the protein phosphatase, calcineurin, in mSOD mice (Li et al., 2004).

5.4 What role does p-Add play in the mSOD mouse and in ALS?

Hyperphosphorylation of p-Add and other phosphoproteins have been found in thoracic spinal cord tissue from patients who died with ALS, compared to controls (Hu et al., 2003). However, the increase in p-Add protein level was the largest of any of the 31 phosphoproteins studied (Hu et al., 2003b). However, no significant difference was found in p-Add protein level in the mSOD mouse compared to controls.

In the mSOD mouse, p-Add immunoreactivity is evident in anatomical regions that are affected in this mutant animal. Phospho-adducin immunoreactivity is found in

motoneurons and their axons, cells of the ventral spinal cord and astrocytes. Furthermore, p-Add immunoreactivity is seen within the vacuolar structures of motoneuron axons that are universally observed in affected animals (Chiu et al., 1995). The immunoreactivity of p-Add is also seen in these same cell types in control animals, although not to the same extent. For example, immunnoreactivity of p-Add is seen in ependymal cells that are not obviously involved in ALS. However, increased regional immunoreactivity of p-Add and an altered subcellular localization pattern of p-Add in neurons is likely associated with the neurodegenerative process leading to cell death.

PKC activation likely exerts cell-specific effects, possibly related to the repertoire of ion channels in different cell types. Adducin phosphorylation in glia probably reflects a re-organization of actin-spectrin interactions in the context of a regenerative response or process extension. These regenerative responses may be triggered by elevations in the protein level and activity of PKC, which is responsible for process extension in some cell types, such as oligodendrocytes (Yoo et al., 1999; Yong et al., 1994). The action of PKC on process extension in astrocytes might be mediated through p-Add, as is the case for changes in platelet shape (Barkalow et al., 2003). However, in neurons, death occurs in cells that express N-methyl-D-aspartate (NMDA) receptors following exposure to phorbol esters that stimulate PKC (Felipo et al., 1993). Use of isoform-specific inhibitors in cell lines transfected with NMDA receptor subunits have shown that a Ca^{2+} and lipid-dependent kinase, likely PKC-β1, is responsible for cell death and acts on the C-terminus of NR2A subunits of the NMDA receptor (Wagey et al., 2001). It is possible that interactions between adducin and the NMDA receptor may be involved in changes of p-Add immunoreactivity in mSOD mice.

5.5 Conclusions and future studies

My study has demonstrated increased immunoreactivity of phosphoadducin in regions of dorsal and ventral grey matter within lumbosacral segments of spinal cord from G93A mSOD mice, compared to controls. The increase in phosphorylation of adducin may provide evidence for aberrant phosphorylation events contributing to motoneuron loss in mSOD mice. The phosphorylation of adducin, although likely a regenerative response in astrocytes, may play an important role in causing neuron death in mSOD mice by affecting the basic structural scaffolding of neuronal dendritic spines and somata. Increased phosphorylation of adducin in nervous tissue may be a useful diagnostic marker in motor neuron diseases. Potentially, similar changes in p-Add immunoreactivity may be present in nervous system tissue from ALS patients.

To explore the role of p-Add in motoneuron death further, it will be interesting to know a) Which intracellular or membrane proteins might interact with p-Add in mSOD mice? b) How these p-Add interacting proteins might be important for causing or preventing motoneuron death in the mSOD mouse model of ALS? To answer these questions, we could use the same mSOD mouse model and primary cultures of neurons or cell lines, co-transfected with cDNA constructs of adducin and other candidate channels/receptors. Specifically, we could examine the co-localization of potential proteins with p-Add in neurons or glial cells by using immunohistochemistical techniques, or identify the physical interaction proteins of p-Add by using biochemical methods such as co-immunoprecipitation or mass spectrometry. Based on many evidence that suggest NMDA receptor and EAAT2 glutamate transporter may involved in the neuronal excitotoxicity of ALS (Duan et al., 1999; Ludolph et al., 2000; Wagey et al.,

2001; Howland et al., 2002) , these two proteins might be good candidates to study. Furthermore, we could perform functional studies by investigating the alteration of surface expression level or membrane potential of channel/receptors in the models described previously, as these changes may have the effects on the motoneuron death of ALS.

Reference List

Ackerley S., Grierson A., Brownlees J., Thornhill P., Anderton B.H., Leigh P.N., Shaw C.E. and Miller C.C. (2000) Glutamate slows axonal transport of neurofilaments in transfected neurons. J Cell Biol.150:165-176.

Ackerley S., Thornhill P., Grierson A.J., Brownlees J., Anderton B.H., Leigh P.N., Shaw C.E. and Miller C.C. (2003) Neurofilament heavy chain side arm phosphorylation regulates axonal transport of neurofilaments. J Cell Biol. 161:489-495.

Ackerley S., Grierson A. J., Banner S., Perkinton M.S., Brownlees J., Byers H.L., Ward M., Thornhill P., Hussain K., Waby J.S., Anderton B.H., Cooper J.D., Dingwall C., Leigh P.N., Shaw C.E. and Miller C.C. (2004) p38alpha stress-activated protein kinase phosphorylates neurofilaments and is associated with neurofilament pathology in amyotrophic lateral sclerosis. Mol. Cell Neurosci. 26, 354-364.

Agar J. and Durham H. (2003) Relevance of oxidative injury in the pathogenesis of motor neuron diseases. Amyotroph Lateral Scler Other Motor Neuron Disord. 4:232-242.

Al-Chalabi A. and Miller C.C. (2003) Neurofilaments and neurological disease. Bioessays. 25:346-355.

Andersen P.M. (2000) Genetic factors in the early diagnosis of ALS. Amyotroph. Lateral Scler. Other Motor Neuron Disord. 1 (Suppl. 1):S31–42

Andersen P.M., Spitsyn V.A., Makarov S.V., Nilsson L., Kravchuk O.I., Bychkovskaya L.S. and Marklund S.L. (2001) The geographical and ethnic distribution of the D90A CuZn-SOD mutation in the Russian Federation. Amyotroph. Lateral Scler. Other Motor Neuron Disord. 2:63–69

Barkalow K. L., Italiano J. E. Jr., Chou D. E., Matsuoka Y., Bennett V. and Hartwig J. H. (2003) Alpha-adducin dissociates from F-actin and spectrin during platelet activation. J. Cell Biol. 161, 557-570.

Beal M.F., Ferrante R.J., Browne S.E., Matthews R.T., Kowall N.W. and Brown R.H.Jr. (1997) Increased 3-nitrotyrosine in both sporadic and familial amyotrophic lateral sclerosis. Ann. Neurol. 42:644–654.

Beckman J.S., Carson M., Smith C.D. and Koppenol W.H. (1993) ALS, SOD and peroxynitrite. Nature 364:584.

Bennett V., Gardner K., and Steiner J.P. (1988) Brain adducin: a protein kinase C substrate that may mediate site-directed assembly at the spectrin-actin junction. J. Biol. Chem. 263:5860–5869.

Bogdanov M.B., Ramos L.E., Xu Z. and Beal M.F. (1998) Elevated hydroxyl radical generation in vivo in an animal model of amyotrophic lateral sclerosis. J. Neurochem. 71:1321–1324.

Borchelt D.R., Lee M.K., Slunt H.S., Guarnieri M., Xu Z.S., Wong P.C., Brown R.H.Jr., Price D.L., Sisodia S.S. and Cleveland D.W. (1994) Superoxide dismutase 1 with mutations linked to familial amyotrophic lateral sclerosis possesses significant activity. Proc. Natl. Acad. Sci. USA 91:8292–8296

Bowling A.C., Barkowski E.E., McKenna-Yasek D., Sapp P., Horvitz H.R., Beal M.F. and Brown R.H. Jr. (1995) Superoxide dismutase concentration and activity in familial amyotrophic lateral sclerosis. J Neurochem. 64:2366-2369.

Bruijn L.I. and Cleveland D.W. (1996) Mechanisms of selective motor neuron death in ALS: insights from transgenic mouse models of motor neuron disease. Neuropathol Appl Neurobiol. 22:373-387.

Bruijn L.I., Beal M.F., Becher M.W., Schulz J.B., Wong P.C., Price D.L. and Cleveland D.W. (1997a) Elevated free nitrotyrosine levels, but not protein-bound nitrotyrosine or hydroxyl radicals, throughout amyotrophic lateral sclerosis (ALS)-like disease implicate tyrosine nitration as an aberrant in vivo property of one familial ALS-linked superoxide dismutase 1 mutant. Proc. Natl. Acad. Sci. USA. 94:7606-7611.

Bruijn L.I., Becher M.W., Lee M.K., Anderson K.L., Jenkins N.A., Copeland N.G., Sisodia S.S., Rothstein J.D., Borchelt D.R., Price D.L. and Cleveland D.W. (1997b) ALS-linked SOD1 mutant G85R mediates damage to astrocytes and promotes rapidly progressive disease with SOD1-containing inclusions. Neuron 18:327-338.

Bruijn L.I., Houseweart M.K., Kato S., Anderson K.L., Anderson S.D., Ohama E., Reaume A.G., Scott R.W. and Cleveland D.W. (1998) Aggregation and motor neuron toxicity of an ALS-linked SOD1 mutant independent from wild-type SOD1. Science. 281:1851-1854.

Bruijn L.I., Miller T.M. and Cleveland D.W. (2004) Unraveling the mechanisms involved in motor neuron degeneration in ALS. Annu Rev Neurosci. 27:723-749.

Brunori M. and Rotilio G. (1984) Biochemistry of oxygen radical species. Methods. Enzymol. 105:22-35.

Chiu A. Y., Zhai P., Dal Canto M. C., Peters T. M., Kwon Y. W., Prattis S. M. and Gurney M. E. (1995) Age-dependent penetrance of disease in a transgenic mouse model of familial amyotrophic lateral sclerosis. Mol. Cell Neurosci. 6:349-362.

Citterio L., Azzani T., Duga S. and Bianchi G. (1999) Genomic organization of the human gamma adducin gene. Biochem. Biophys. Res. Commun. 266:110–114.

Cleveland D.W. (1999). From Charcot to SOD1: mechanisms of selective motor neuron death in ALS. Neuron. 24:515–520.

Collard J.F., Cote F. and Julien J.P. (1995) Defective axonal transport in a transgenic mouse model of amyotrophic lateral sclerosis. Nature. 375:61-64.

Dal Canto M.C. and Gurney M.E. (1997) A low expressor line of transgenic mice carrying a mutant human Cu,Zn superoxide dismutase (SOD1) gene develops pathological changes that most closely resemble those in human amyotrophic lateral sclerosis. Acta Neuropathol (Berl). 93:537-550.

Derick L.H., Liu C.S., Chishti A.H. and Palek J. (1992) Protein immunolocalization in the spread erythrocyte membrane skeleton. Eur. J. Cell Biol. 57:317–320.

Dong L., Chapline C., Mousseau B., Fowler L., Ramsay K., Stevens J. L. and Jaken S. (1995) 35H, a sequence isolated as a protein kinase C binding protein, is a novel member of the adducin family. J. Biol. Chem. 270: 25534–25540.

Duan S., Anderson C.M., Stein B.A. and Swanson R.A. (1999) Glutamate induces rapid upregulation of astrocyte glutamate transport and cell-surface expression of GLAST. J Neurosci. 19:10193-10200.

Durham H.D., Roy J., Dong L. and Figlewicz D.A. (1997) Aggregation of mutant Cu/Zn superoxide dismutase proteins in a culture model of ALS. J Neuropathol Exp Neurol. 56:523-530.

Eisen A. and Krieger C. (1998) Amyotrophic lateral sclerosis: A synthesis of research and clinical practice. Cambridge, UK. 303 pp.

Farah C. A., Nguyen M. D., Julien J. P. and Leclerc N. (2003) Altered levels and distribution of microtubule-associated proteins before disease onset in a mouse model of amyotrophic lateral sclerosis. J. Neurochem. 84:77-86.

Felipo V., Minana M. D. and Grisolia S. (1993) Inhibitors of protein kinase C prevent the toxicity of glutamate in primary neuronal cultures. Brain Res. 604:192-196.

Ferrante R.J., Shinobu L.A., Schulz J.B., Matthews R.T., Thomas C.E., Kowall N.W., Gurney M.E. and Beal M.F. (1997a) Increased 3-nitrotyrosine and oxidative damage in mice with a human copper/zinc superoxide dismutase mutation. Ann. Neurol. 42:326-334.

Ferrante R.J., Browne, S.E., Shinobu, L.A., Bowling, A.C., Baik, M.J., MacGarvey, U., Kowall, N.W., Brown Jr., R.H. and Beal, M.F., (1997b). Evidence of increased oxidative damage in both sporadic and familial amyotrophic lateral sclerosis. J. Neurochem. 69:2064–2074.

Fukata Y., Oshiro N., Kinoshita N., Kawano Y., Matsuoka Y., Bennett V., Matsuura Y. and Kaibuchi K. (1999) Phosphorylation of adducin by Rho-kinase plays a crucial role in cell motility. J. Cell Biol. 145:347–361

Gardner K. and Bennett V. (1987) Modulation of spectrin-actin assembly by erythrocyte adducin. Nature. 328:359–362.

Ghassemi F., Dib-Hajj S.D. and Waxman S.G. (2001) Beta1 adducin gene expression in DRG is developmentally regulated and is upregulated by glial-derived neurotrophic factor and nerve growth factor. Brain Res. Mol. Brain Res. 90:118-124.

Gilligan D.M., Lieman J. and Bennett V. (1995) Assignment of the human beta-adducin gene (ADD2) to 2p13–p14 by in situ hybridization. Genomics 28: 610–612

Gilligan D.M., Lozovatsky L. and Silberfein A. (1997) Organization of the human beta-adducin gene (ADD2). Genomics. 43:141-148.

Gilligan D.M., Lozovatsky L., Gwynn B., Brugnara C., Mohandas N. and Peters L. L.(1999) Targeted disruption of the beta adducin gene (Add2) causes red blood cell spherocytosis in mice. Proc. Natl. Acad. Sci. USA 96:10717–10722.

Gilligan D.M., Sarid R. and Weese J. (2002) Adducin in platelets: activation-induced phosphorylation by PKC and proteolysis by calpain. Blood. 99:2418-2426.

Goldberg Y.P., Lin B.Y., Andrew S.E., Nasir J., Graham R., Glaves M.L., Hutchinson G., Theilmann J., Ginzinger D.G. and Schappert K. (1992) Cloning and mapping of the alpha-adducin gene close to D4S95 and assessment of its relationship to Huntington disease. Hum Mol Genet. 1:669-675.

Gurney M.E., Pu H., Chiu A.Y., Dal Canto M.C., Polchow C.Y., Alexander D.D., Caliendo J., Hentati A., Kwon Y.W. and Deng H.X. (1994) Motor neuron degeneration in mice that express a human Cu, Zn superoxide dismutase mutation. Science 264:1772-1775.

Haenggeli C. and Kato A.C. (2002) Differential vulnerability of cranial motoneurons in mouse models with motor neuron degeneration. Neurosci Lett. 335:39-43.

Hall E. D., Oostveen J. A. and Gurney M.E. (1998) Relationship of microglial and astrocytic activation to disease onset and progression in a transgenic model of familial ALS. Glia. 23:249-256.

Hamson D.K., Hu J.H., Krieger C. and Watson N.V. (2002) Lumbar motoneuron fate in a mouse model of amyotrophic lateral sclerosis. NeuroReport. 13:2291-2294.

Hirano A., Nakano I., Kurland L.T., Mulder D.W., Holley P.W. and Saccomanno G. (1984) Fine structural study of neurofibrillary changes in a family with amyotrophic lateral sclerosis. J Neuropathol Exp Neurol. 43:471-480.

Howland D.S., Liu J., She Y., Goad B., Maragakis N.J., Kim B., Erickson J., Kulik J., DeVito L., Psaltis G., DeGennaro L.J., Cleveland D.W. and Rothstein J.D. (2002) Focal loss of the glutamate transporter EAAT2 in a transgenic rat model of SOD1 mutant-mediated amyotrophic lateral sclerosis (ALS). Proc Natl Acad Sci U S A. 99:1604-1609

Hu J.H., Chernoff K., Pelech S. and Krieger C. (2003a) Protein kinase and protein phosphatase expression in the CNS of G93A mSOD over-expressing mice. J. Neurochem. 85:422-431.

Hu J.H., Zhang H., Wagey R., Krieger C. and Pelech S.L. (2003b) Protein kinase and protein phosphatase expression in amyotrophic lateral sclerosis spinal cord. J. Neurochem. 85:432-442.

Hughes C.A. and Bennett V. (1995) Adducin: a physical model with implication for function in assembly of spectrin-actin complexes. J. Biol. Chem. 270:18990–18996.

Johnston J.A., Dalton M.J., Gurney M.E. and Kopito R.R. (2000) Formation of high molecular weight complexes of mutant Cu, Zn-superoxide dismutase in a mouse model for familial amyotrophic lateral sclerosis. Proc Natl Acad Sci U S A. 97:12571-12576.

Joshi R. and Bennett V. (1990) Mapping the domain structure of human erythrocyte adducin. J. Biol. Chem. 265:13130–13136.

Joshi R., Gilligan D.M., Otto E., McLaughlin T. and Bennett V. (1991) Primary structure and domain organization of human alpha and beta adducin. J. Cell Biol. 115:665–675.

Julien J.P. (2001) Amyotrophic lateral sclerosis. unfolding the toxicity of the misfolded. Cell. 104:581-591.

Jung C., Yabe J.T. and Shea T.B. (2000) C-terminal phosphorylation of the high molecular weight neurofilament subunit correlates with decreased neurofilament axonal transport velocity. Brain Res. 856:12-19.

Kaiser H.W., O'Keefe E. and Bennett V. (1989) Adducin: Ca++-dependent association with sites of cell–cell contact. J. Cell Biol. 109:557–569.

Katagiri T., Ozaki K., Fujiwara T., Shimizu F., Kawai A., Okuno S., Suzuki M., Nakamura Y., Takahashi E. and Hirai Y. (1996) Cloning, expression and chromosome mapping of adducin-like 70 (ADDL), a human cDNA highly homologous to human erythrocyte adducin. Cytogenet Cell Genet. 74:90-95.

Kimura K., Fukata Y., Matsuoka Y., Bennett V., Matsuura Y., Okawa K., Iwamatsu A. and Kaibuchi K. (1998) Regulation of the association of adducin with actin filaments by Rho-associated kinase (Rho-kinase) and myosin phosphatase. J. Biol. Chem. 273:5542–5548.

Krieger C., Lanius R.A., Pelech S.L. and Shaw C.A. (1996) Amyotrophic lateral sclerosis: the involvement of intracellular Ca2+ and protein kinase C. Trends Pharmacol Sci. 17:114-120.

Krieger C., Hu J.H., and Pelech S. (2003) Aberrant protein kineses and phosphoproteins in amyotrophic lateral sclerosis. Trends Pharmacol. Sci. 24:535-541.

Kuhlman P.A., Hughes C.A., Bennett V. and Fowler V.M. (1996) A new function for adducin, calcium calmodulin regulated capping of the barbed ends of actin filaments. J. Biol. Chem. 271:7986–7991.

Lanius R.A., Paddon H.B., Mezei M., Wagey R., Krieger C., Pelech S. L. and Shaw C.A. (1995) A role for amplified protein kinase C activity in the pathogenesis of amyotrophic lateral sclerosis. J. Neurochem. 65:927-930.

Li S., Wang X., Klee C.B. and Krieger C. (2004) Overexpressed mutant G93A superoxide dismutase protects calcineurin from inactivation. Brain Res. Mol. Brain Res. 125:156-161.

Li X., Matsuoka Y. and Bennett V. (1998) Adducin preferentially recruits spectrin to the fast-growing ends of actin filaments in a complex requiring the MARCKS-related domain and a newly defined oligomerization domain. J. Biol. Chem. 273:19329-19338.

Lin B., Nasir J., McDonald H., Graham R., Rommens J.M., Goldberg Y.P. and Hayden M.R. (1995) Genomic organization of the human alpha-adducin gene and its alternately spliced isoforms. Genomics 25: 93–99.

Ludolph A.C., Meyer T. and Riepe M.W. (2000) The role of excitotoxicity in ALS--what is the evidence? J Neurol. 247 Suppl 1:I7-16.

Matsuoka Y., Hughes C.A. and Bennett V. (1996) Adducin regulation. Definition of the calmodulin-binding domain and sites of phosphorylation by protein kinases A and C. J Biol. Chem. 271:25157–25166.

Matsuoka Y., Li X. and Bennett V. (1998) Adducin is an in vivo substrate for protein kinase C: phosphorylation in the MARCKS-related domain inhibits activity in promoting spectrin–actin complexes and occurs in many cells, including dendritic spines of neurons. J. Cell Biol. 142:485-497.

McCord J.M. and Fridovich I. (1969) The utility of superoxide dismutase in studying free radical reactions. I. Radicals generated by the interaction of sulfite, dimethyl sulfoxide, and oxygen. J Biol Chem. 244:6056-6063.

McMahon S.S. and McDermott K.W. (2002) Morphology and differentiation of radial glia in the developing rat spinal cord. J. Comp. Neurol. 454, 263-271.

Mische S.M., Mooseker M.S. and Morrow J.S. (1987) Erythrocyte adducin: a calmodulin-regulated actin-bundling protein that stimulates spectrin–actin binding. J. Cell Biol. 105:2837–2845.

Mohajeri M.H., Figlewicz D.A. and Bohn M.C. (1998) Selective loss of alpha motoneurons innervating the medial gastrocnemius muscle in a mouse model of amyotrophic lateral sclerosis. Exp. Neurol. 150:329-336.

Nguyen M.D., Lariviere R.C. and Julien J.P. (2001) Deregulation of Cdk5 in a mouse model of ALS: toxicity alleviated by perikaryal neurofilament inclusions. Neuron. 30:135-147.

Nobes C. and Hall A. (1994) Regulation and function of the Rho subfamily of small GTPases. Curr Opin Genet Dev. 4:77-81.

Parekh D.B., Ziegler W. and Parker P.J. (2000) Multiple pathways control protein kinase C phosphorylation. EMBO J. 19:496-503.

Pramatarova A., Laganiere J., Roussel J., Brisebois K. and Rouleau G.A. (2001) Neuron-specific expression of mutant superoxide dismutase 1 in transgenic mice does not lead to motor impairment. J. Neurosci. 21:3369-3374.

Price D.L., Wong P.P., Markowska A.L., Lee M.K., Thinakaren G., Cleveland D.W., Sisodia S.S. and Borchelt D.R. (2000) The value of transgenic models for the study of neurodegenerative diseases, Ann. NY Acad. Sci. 920:179–191.

Rakic P. (2003) Elusive radial glial cells: historical and evolutionary perspective. Glia. 43:19-32.

Reaume A.G., Elliott J.L., Hoffman E.K., Kowall N.W., Ferrante R.J., Siwek D.F., Wilcox H.M., Flood D.G., Beal M.F., Brown R.H. Jr, Scott R.W. and Snider W.D. (1996) Motor neurons in Cu/Zn superoxide dismutase-deficient mice develop normally but exhibit enhanced cell death after axonal injury. Nat Genet. 13:43-47.

Ridley A.J. and Hall A. (1992) The small GTP-binding protein rho regulates the assembly of focal adhesions and actin stress fibers in response to growth factors. Cell. 70:389-399.

Ridley A.J. (1996) Rho: theme and variations. Curr Biol. 6:1256-1264.

Robberecht W., Sapp P., Viaene M.K., Rosen D., McKenna-Yasek D., Haines J., Horvitz R., Theys P. and Brown R. Jr. (1994) Cu/Zn superoxide dismutase activity in familial and sporadic amyotrophic lateral sclerosis. J Neurochem. 62:384-387.

Rosen D., Siddique T., Patterson D., Figlewicz D.A., Sapp P., Hentati A., Donaldson D., Goto J., O'Regan J.P. and Deng H.X. (1993) Mutations in Cu/Zn superoxide dismutase gene are associated with familial amyotrophic lateral sclerosis. Nature. 362:59-62.

Rosenmund C. and Westbrook G.L. (1993) Calcium-induced actin depolymerizationreduces NMDA channel activity. Neuron. 10:805– 814.

Rothstein J.D., Bristol L.A., Hosler B., Brown R.H.Jr. and Kuncl R.W. (1994) Chronic inhibition of superoxide dismutase produces apoptotic death of spinal neurons. Proc Natl Acad Sci U S A. 91:4155-4159.

Rouleau G.A., Clark A.W., Rooke K., Pramatarova A., Krizus A., Suchowersky O., Julien J.P. and Figlewicz D. (1996) SOD1 mutation is associated with accumulation of neurofilaments in amyotrophic lateral sclerosis. Ann Neurol. 39:128-131.

Schmidt M.L., Carden M.J., Lee V.M. and Trojanowski J.Q. (1987) Phosphate dependent and independent neurofilament epitopes in the axonal swellings of patients with motor neuron disease and controls. Lab Invest. 56:282-294.

Seidel B., Zuschratter W., Wex H., Garner C.C. and Gundelfinger E.D. (1995) Spacial and sub-cellular localization of the membrane cytoskeleton-associated protein alpha-adducin in the rat brain. Brain Res. 700:13–24.

Shibata N., Hirano A., Kobayashi M., Siddique T., Deng H.X., Hung W.Y., Kato T. and Asayama K. (1996) Intense superoxide dismutase-1 immunoreactivity in intracytoplasmic hyaline inclusions of familial amyotrophic lateral sclerosis with posterior column involvement. J Neuropathol Exp Neurol. 55:481-490.

Shima T., Okumura N., Takao T., Satomi Y., Yagi T., Okada M. and Nagai K. (2001) Interaction of the SH2 domain of Fyn with a cytoskeletal protein, beta-adducin. J. Biol. Chem. 276:42233-42240.

Sobue G., Hashizume Y., Yasuda T., Mukai E., Kumagai T., Mitsuma T. and Trojanowski J.Q. (1990) Phosphorylated high molecular weight neurofilament protein in lower motor neurons in amyotrophic lateral sclerosis and other neurodegenerative diseases involving ventral horn cells. Acta Neuropathol (Berl). 79:402-408.

Strong M.J., Sopper, M.M., Crow, J.P., Strong, W.L. and Beckman, J.S., (1998). Nitration of the low molecular weight neurofilament is equivalent in sporadic amyotrophic lateral sclerosis and control cervical spinal cord. Biochem. Biophys. Res. Commun. 248:157–164.

Suriyapperuma S.P., Lozovatsky L., Ciciotte S.L., Peters L.L. and Gilligan D.M. (2000) The mouse adducin gene family: alternative splicing and chromosomal localization Mamm. Genome. 11:16–23.

Tisminetzky S., Devescovi G., Tripodi G., Muro A., Bianchi G., Colombi M., Moro L., Barlati S., Tuteja R. and Baralle F.E. (1995) Genomic organisation and chromosomal localisation of the gene encoding human beta adducin. Gene. 167:313-316.

Troy C.M. and Shelanski M.L. (1994) Down-regulation of copper/zinc superoxide dismutase causes apoptotic death in PC12 neuronal cells. Proc Natl Acad Sci U S A. 91:6384-6387.

Tsukagoshi H., Yanagisawa N., Oguchi K., Nagashima K. and Murakami T. (1979) Morphometric quantification of the cervical limb motor cells in controls and in amyotrophic lateral sclerosis. J. Neurol. Sci. 41:287-297.

Tu P.H., Raju P., Robinson K.A., Gurney M.E., Trojanowski J.Q. and Lee V.M. (1996) Transgenic mice carrying a human mutant superoxide dismutase transgene develop neuronal cytoskeletal pathology resembling human amyotrophic lateral sclerosis lesions. Proc Natl Acad Sci USA. 93:3155-3160.

Wagey R., Krieger C. and Shaw C.A. (1997) Abnormal dephosphorylation effect on NMDA receptor regulation in ALS spinal cord. Neurobiol. Dis. 4:350-355.

Wagey R., Hu J., Pelech S.L., Raymond L.A. and Krieger C. (2001) Modulation of NMDA-mediated excitotoxicity by protein kinase C. J. Neurochem. 78:715-726.

Wang J., Xu G. and Borchelt D.R. (2002) High molecular weight complexes of mutant superoxide dismutase 1: age-dependent and tissue-specific accumulation, Neurobiol. Dis. 9:139–148.

Watson R.E., Wiegland S.J., Clough R.W. and Hoffman G.E., (1986) Use of cryoprotectant to maintain long-term peptide immunoreactivity and tissue morphology, Peptides 7:155–159.

Wiedau-Pazos M., Goto J.J., Rabizadeh S., Gralla E.B., Roe J.A., Lee M.K., Valentine J.S. and Bredesen D.E. (1996) Altered reactivity of superoxide dismutase in familial amyotrophic lateral sclerosis. Science. 271:515-518.

Williamson T.L., Corson L.B., Huang L., Burlingame A., Liu J., Bruijn L.I. and Cleveland D.W. (2000) Toxicity of ALS-linked SOD1 mutants. Science. 288:399

Williamson T.L. and Cleveland D.W. (1999) Slowing of axonal transport is a very early event in the toxicity of ALS-linked SOD1 mutants to motor neurons. Nat Neurosci. 2:50-56.

Wong P.C., Pardo C.A., Borchelt D.R., Lee M.K., Copeland N.G., Jenkins N.A., Sisodia S.S., Cleveland D.W. and Price D.L. (1995) An adverse property of a familial ALS-linked SOD1 mutation causes motor neuron disease characterized by vacuolar degeneration of mitochondria. Neuron. 14:1105-1116.

Wyneken U., Smalla K.H., Marengo J.J, Soto D., de la Cerda A., Tischmeyer W., Grimm R., Boeckers T.M., Wolf G., Orrego F. and Gundelfinger E.D. (2001) Kainate-induced seizures alter protein composition and N-methyl-D-aspartate receptor function of rat forebrain postsynaptic densities. Neuroscience. 102:65-74.

Yang W., Sopper M.M., Leystra-Lantz C. and Strong M.J. (2003) Microtubule-associated tau protein positive neuronal and glial inclusions in ALS. Neurology. 61:1766-1773.

Yong V.W., Dooley N.P. and Noble P.G. (1994) Protein kinase C in cultured adult human oligodendrocytes: a potential role for isoform alpha as a mediator of process outgrowth. J. Neurosci. Res. 39:83-96.

Yoo A.S., Krieger C. and Kim S.U. (1999) Process extension and intracellular Ca2+ in cultured murine oligodendrocytes. Brain Res. 827:19-27.

Zang D.W. and Cheema S.S. (2002) Degeneration of corticospinal and bulbospinal systems in the superoxide dismutase 1(G93A G1H) transgenic mouse model of familial amyotrophic lateral sclerosis. Neurosci Lett. 332:99-102.